Article:
Jaffar, MM, Nahil, MA and Williams, PT orcid.org/0000-0003-0401-9326 (2020) Synthetic natural gas production from the three stage (i) pyrolysis (ii) catalytic steam reforming (iii) catalytic hydrogenation of waste biomass. Fuel Processing Technology, 208. 106515. ISSN 0378-3820

https://doi.org/10.1016/j.fuproc.2020.106515

Synthetic Natural Gas Production from the Three Stage (i) Pyrolysis (ii) Catalytic Steam Reforming (iii) Catalytic Hydrogenation of Waste Biomass

Mohammad M. Jaffar, Mohamad A. Nahil, Paul T. Williams*
School of Chemical and Process Engineering, University of Leeds, Leeds, LS2 9JT, U.K.
(*Corresponding author; Email; p.t.williams@leeds.ac.uk; Tel; #44 1133432504)

Abstract:

Synthetic natural gas (methane) production was systematically investigated by optimising various operating parameters using a three stage (i) biomass pyrolysis (ii) catalytic steam reforming (iii) catalytic hydrogenation reactor system. Several operating parameters were optimized including catalytic steam reforming temperature, steam weight hourly space velocity (WHSV), catalytic hydrogenation temperature and hydrogen gas space velocity. In addition, the influence of different metal catalysts (Ni/Al_2O_3, Fe/Al_2O_3, Co/Al_2O_3, and Mo/Al_2O_3), catalyst calcination temperature, catalyst metal loadings, and different catalyst support materials (Al_2O_3, SiO_2, and MCM-41) was carried out specifically to optimize catalytic hydrogenation in the third stage reactor. The highest methane yield of 13.73 mmoles $g^{-1}_{biomass}$ (22.02 g CH_4 100 $g^{-1}_{biomass}$) was obtained with a second stage catalytic steam reforming temperatureof 800 °C over a 10 wt.% Ni/Al_2O_3 catalyst and with a steam WHSV of 5 mL h^{-1} $g^{-1}_{catalyst}$ together with a third stage catalytic hydrogenation temperature of 350 °C over a 10 wt.% Ni/Al_2O_3 catalyst with added hydrogen gas space velocity of 2400 mL h^{-1} $g^{-1}_{catalyst}$.

Keywords: Biomass; Methane; Pyrolysis; Reforming; Methanation

1. INTRODUCTION.

With increased global energy demand and the associated pollution problems, there is even greater interest in the development of sustainable routes to manage energy demand without causing any harm to the environment [1]. Studies have focussed on the substitution of fossil fuels with lignocellulosic biomass because it is not only abundant in nature but also it is a renewable source of energy and a carbon-neutral fuel [2]. Of great interest are processes that can convert biomass into fuels that can directly substitute into the petroleum refining infrastructure or the natural gas infrastructure rather than trying to develop a new bioenergy infrastructure. Methane production from biomass is an attractive option because of the already well developed and organized infrastructure and distribution facilities for natural gas. Methane production from biomass may be carried out via a thermochemical pathway. To recover energy from biomass, thermochemical methods such as pyrolysis may be employed [3, 4]. Pyrolysis is the thermal degradation of biomass in the absence of an oxidizing agent and results in the formation of solid, liquid and gaseous products. We have reported previously on the optimisation of a two-stage, pyrolysis-catalytic hydrogenation process for the production of methane from biomass [19]. This paper progresses that work by the introduction of an additional reaction stage to produce a three stage (i) pyrolysis (ii) catalytic steam reforming (iii) catalytic hydrogenation reactor system for the production of methane from biomass. The aim of this process is to completely convert the oxygenated and non-oxygenated hydrocarbon produced as the result of biomass pyrolysis (1^{st} stage) into carbon oxides and hydrogen in a catalytic steam reforming reactor (2^{nd} stage) and then to convert this product gaseous mixture into methane in the presence of added hydrogen in a catalytic hydrogenation reactor (3^{rd} stage). This process involves the series of reactions as shown in Table 1. During the pyrolysis of biomass, thermal degradation takes place and results in the formation of solid char, gaseous products, and oxygenated and non-oxygenated hydrocarbons

(eq. 1). These gaseous products and oxygenated and non-oxygenated hydrocarbons undergo a series of reactions in the catalytic steam reforming reactor (eq. 2 to eq. 9). For example, oxygenated hydrocarbons undergo catalytic cracking reactions and result in the formation of carbon oxides, hydrogen and non-oxygenated hydrocarbons (eq. 2). Catalytic steam reforming and dry reforming of oxygenated and non-oxygenated hydrocarbons result in the formation of carbon monoxide and hydrogen (eq. 3 to eq. 6). Since a significant amount of carbon monoxide is produced from steam and dry reforming reactions, it reacts with the added steam and undergoes water gas shift reaction and results in the formation of carbon dioxide and hydrogen (eq. 7). Also, at higher temperature ranges, there is the possibility of Boudouard reaction and carbon steam gasification reactions (eq. 8 and eq. 9). The product gases from the catalytic steam reforming reactor are mainly composed of carbon oxides and hydrogen. This product gaseous mixture upon entering the catalytic hydrogenation reactor undergoes methanation reactions and carbon hydrogasification reactions and results in the formation of methane gas (eq. 10 to eq. 12).

Optimization studies of catalytic steam reforming show that this process takes place at high temperature ranges (700 - 1000 °C) in the presence of catalysts [5]. Different catalysts have been studied to enhance the catalytic steam reforming process. Among the different metal catalysts, noble metals such as Pt, Rh, Ru and Pd showed promising results but because of their higher costs these metals are not commonly used [6-8]. Ni metal based catalysts because of their cost-effectiveness and high catalytic activity are used on a commercial scale [9]. Also, different support materials such as Al_2O_3, SiO_2, MCM-41, zeolites, and dolomite etc. have been reported in the literature to be active for steam reforming reactions [5, 10-13]. However, Al_2O_3 support material is preferred because of its high stability [14]. Therefore Ni metal loaded on Al_2O_3 support has been employed in the catalytic steam reforming process.

However, catalytic hydrogenation for carbon oxides conversion (methanation reactions eq 10 - eq 11) takes place at a lower temperature range of around 200 - 500 °C. Several catalytic studies have been reported to enhance methane yield by carbon oxides hydrogenation using heterogeneous VIII-B group metals such as Ni, Fe, Co, Ru, Rh, Pt and Pd over various support materials such as TiO_2, SiO_2, ZrO_2, Al_2O_3, and CeO_2. Metals such as Ru, Rh, and Ni based catalysts have been reported to be active hydrogenation catalysts [15-18]. But because of the lower cost, high activity and selectivity towards the methanation reaction, Ni metal based catalysts have received most attention. In addition, among the different catalytic support materials used, Al_2O_3 support shows higher stability resulting in enhanced catalytic activity [15]. Therefore, in this work Ni metal over alumina support material has been incorporated for the initial optimization of catalytic hydrogenation operating parameters.

In this article, we report on the optimization of various operating parameters for the (i) pyrolysis (ii) catalytic steam reforming of biomass to maximize the conversion of higher molecular weight hydrocarbons derived from biomass pyrolysis into carbon oxides and hydrogen as feedstock for catalytic hydrogenation. The parameters investigated were, catalytic steam reforming temperature, steam WHSV, catalytic hydrogenation temperature, and hydrogen gas space velocity. This was followed by the investigation of the three stage (i) pyrolysis (ii) catalytic steam reforming (iii) catalytic hydrogenation reactor system where the effect of different metal catalysts, influence of catalyst calcination temperature, different catalyst metal loadings and different support materials was investigated.

2. MATERIALS AND METHODS.

2.1 Biomass Sample.

The waste biomass feedstock used in the experiments was waste wood sawdust which was compressed to form wood pellets. The biomass feedstock was obtained from Liverpool Wood Pellets Ltd., Liverpool, UK. These wood pellets were crushed and sieved to obtain the particle size of 0.3 to 0.5 mm. The elemental analysis was performed using a Vario Micro elemental analyser and showed a hydrogen content of 5.4 wt.%, carbon content of 50.1 wt.%, nitrogen content of 0.1 wt.% and oxygen content of 48.6 wt.%. The proximate analysis of the biomass was performed using a Shimadzu TGA-50 thermogravimetric analyser and showed that the biomass feedstock consisted of 93.3 wt.% volatiles, 7.8 wt.% moisture, 0.3 wt.% ash and 6.7 wt.% fixed carbon.

2.2 Catalyst Preparation.

The catalyst used for the optimization of the (i) pyrolysis (ii) catalytic steam reforming reactor system for biomass processing was a 10 wt.% Ni loaded on alumina (Al_2O_3) support and was prepared by using a wet impregnation method. To prepare the catalyst, 10 wt. % of Ni using nickel nitrate hexahydrate was dissolved in 25 ml of deionized water with continuous stirring for 30 min to obtain an aqueous solution. Alumina support was then added into this aqueous solution, stirred for 30 min, and then heated continuously with 15 °C rise in temperature after every 30 min until all the water evaporated leaving behind a semi solid slurry. This semi-solid slurry was then dried overnight at 105 °C in an oven. The dried sample was then calcined in a furnace at 750 °C with heating rate of 20 °C min^{-1} for 3 h. The

calcined catalyst was then crushed and sieved to obtain a particle size range of 50-212 μm. Finally, the sieved catalyst was reduced in a H_2 atmosphere (5% H_2, and 95 % N_2) at 800 °C for 2 h in a reduction furnace.

The catalysts used for catalytic hydrogenation in the three stage (i) pyrolysis (ii) catalytic steam reforming (iii) catalytic hydrogenation reactor system were each prepared using the same wet impregnation method described above. Different, metal catalysts (10 wt. % of Ni, Fe, Co, and Mo) on alumina support were investigated in the catalytic hydrogenation reactor. Nickel nitrate hexahydrate (Sigma-Aldrich, 99.99 %), cobalt nitrate hexahydrate (Sigma-Aldrich, 99.99 %), iron (III) nitrate nonahydrate (Sigma-Aldrich, 99.95 %), and ammonium molybdate (para) tetrahydrate (Alfa Aesar, 99. 0%) were used to load the active metal over the alumina support. All of these catalysts after impregnation were dried, calcined, crushed and sieved as before to produce the catalyst particle size of 50-212 μm then reduced in the H_2 atmosphere.

In addition, the influence of catalyst support material was investigated for the catalytic hydrogenation reactor, using SiO_2 and MCM-41 in addition to the Al_2O_3, all with nickel as the active catalyst metal. SiO_2 and MCM-41 was added to the aqueous solution of nickel nitrate hexahydrate to obtain 10 wt.% Ni/SiO_2 and 10 wt.% Ni/MCM-41 in addition to the prepared Ni/Al_2O_3. For the study of catalyst support material, the prepared aqueous solution was dried and calcined at 950 °C (rather than 750 °C) for 3h. As before, the calcined catalysts were crushed and sieved to obtain the particle size of 50-212 μm and reduced under H_2 atmosphere at 800 °C for 2 h.

146 **2.3. Three stage (i) pyrolysis (ii) catalytic steam reforming (iii) catalytic hydrogenation**
147 **reactor system.**

148 The three stage (i) pyrolysis (ii) catalytic steam reforming (iii) catalytic hydrogenation
149 experimental reactor system used for methane production from biomass is shown in Figure 1
150 as a schematic diagram.

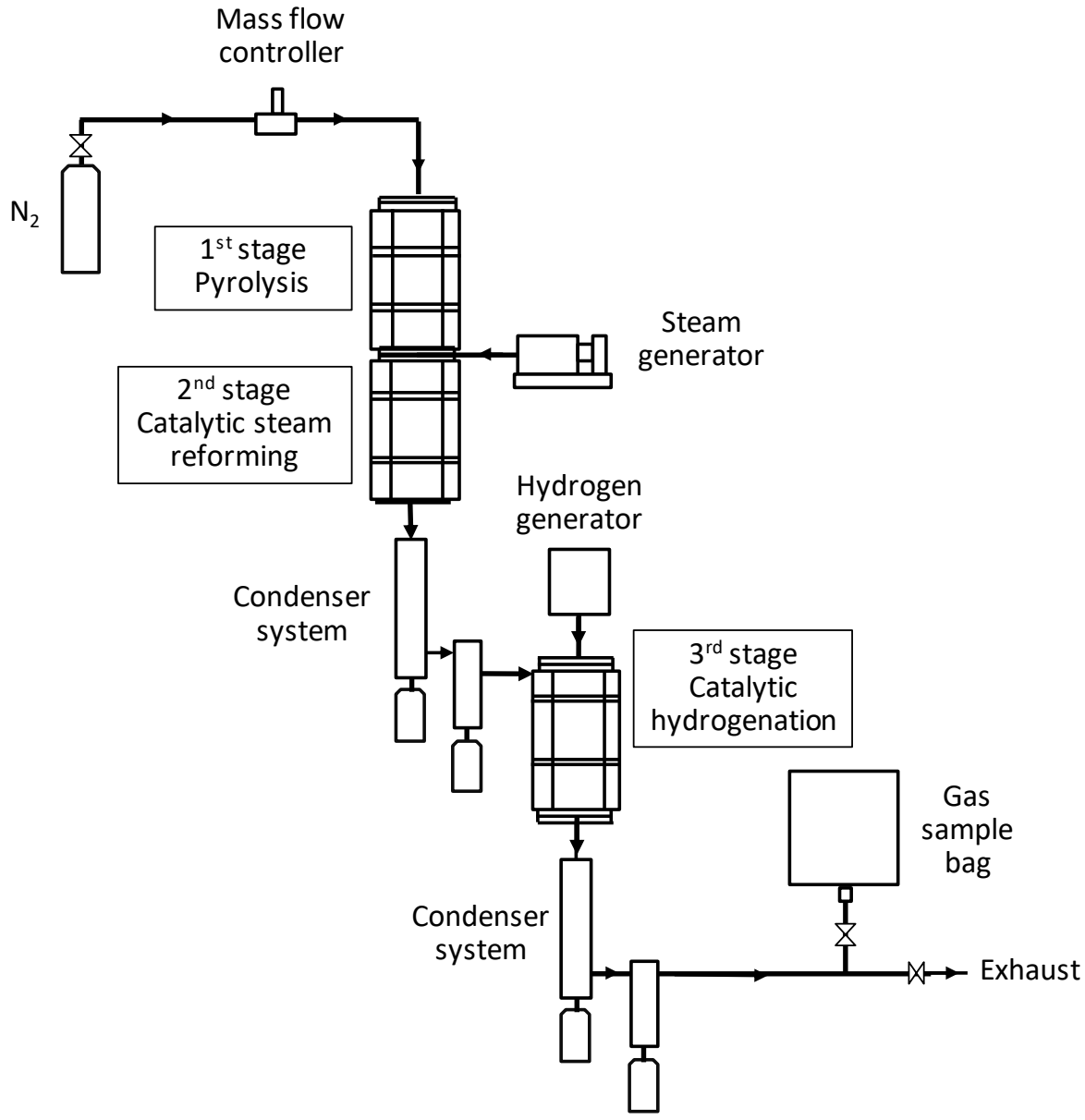

151

152 **Figure 1.** Schematic diagram of the three stage (i) pyrolysis (ii) catalytic steam reforming
153 (iii) catalytic hydrogenation reactor system.

154

Pyrolysis of the biomass was carried out in the first stage of the reactor which was constructed of stainless steel having dimensions of 25 cm long x 5 cm diameter and heated externally by separate electrical furnaces. A biomass sample weight of 1.0 gm was placed in a crucible and suspended in the centre of the pyrolysis reactor. Evolved pyrolysis volatiles were transferred directly to the 2nd stage catalytic steam reforming reactor where 1.0 gm of 10 wt. % Ni/Al_2O_3 catalyst was held in place using stainless steel mesh and quartz wool. The 2nd stage catalytic steam reforming reactor was constructed of stainless steel having dimensions of 32 cm long x 2 cm diameter externally heated by an electrical furnace. Hydrocarbon volatiles and gases from pyrolysis undergo catalytic cracking, gasification reactions and steam reforming in the presence of added steam in the 2nd stage reactor. Product gases derived from the catalytic steam reforming reactor passed through a condensation system to remove condensable products (almost entirely water and traces of bio-oil) then transferred to the 3rd stage catalytic hydrogenation reactor which was constructed of stainless steel with dimensions of 14.5 cm long x 2 cm diameter externally heated by an electrical furnace. Dry ice condensers were used at the output of the catalytic hydrogenation reactor to condense the water produced as the result of methanation reaction. The final gaseous product was collected in 25 L Tedlar gas sample bag. All of the three reactors were temperature controlled and monitored to the desired temperatures. Nitrogen was used as a carrier gas to purge product gases through the reactor system. Steam was injected directly into the 2nd stage steam reforming reactor using a WPI SPLG100 syringe pump. Hydrogen for the 3rd stage catalytic hydrogenation was produced and supplied using a Packard 9200 H_2 generator.

The experimental procedure consisted of, pre-heating of the 2nd stage catalytic steam reforming reactor and the 3rd stage catalytic hydrogenation reactor to the desired temperature. Once the required temperatures were achieved and stabilized, the pyrolysis reactor was then heated from ambient temperature to 800 °C at a heating rate of 20 °C min^{-1}. Once the

pyrolysis reactor started heating, steam injection to the reforming reactor and H_2 addition to the hydrogenation reactor commenced. Baseline experiments were carried out using quartz sand for comparison with the catalyst. For accuracy purposes repeatability and reproducibility tests were performed and negligible difference was observed.

Initial experiments used only the (i) pyrolysis and (ii) catalytic steam reforming of biomass to investigate the influence of catalytic steam reforming temperature, and steam WHSV on the production of carbon oxides and hydrogen. This was then followed by the investigation of the full three stage (i) pyrolysis (ii) catalytic steam reforming (iii) catalytic hydrogenation reactor system, concentrating on the influence of metal catalysts, catalyst calcination temperature, amount of catalyst metal loadings and different support materials.

2.4. Gas analysis

The non-condensable gas product obtained in the Tedlar gas sample bag was analysed immediately after each experiment using packed column gas chromatography. Hydrocarbon gases ranging from C_1 to C_4 were analysed using a Varian CP 3380 with flame ionization detector, 2 m long x 2 mm diameter chromatographic column with 80-100 mesh HayeSep packing and N_2 as a carrier gas. Permanent gases, H_2, O_2, N_2, and CO were analysed using a Varian CP 3330 GC having a thermal conductivity detector, a 2 m long x 2 mm diameter chromatographic column with 60 – 80 mesh HayeSep packing and Ar as gas carrier. CO_2 was analysed by using a Varian CP 3330 GC having thermal conductivity detector, a 2 m long x 2 mm diameter chromatographic column with 80-100 mesh Restek packing.

2.5. Catalyst characterization.

The metal type and the metal particle size analysis of the prepared catalysts were carried out using an XPERT X-ray diffractometer having Cu Kα radiation operated at 40kV and 40mA. Peaks of the catalysts were identified by using a High Score plus software package with built in program for metallic size calculation using the Scherrer equation. In addition, the morphology of the catalysts was studied by using an Hitachi SU8230 scanning electron microscope (SEM) operated at 20kV coupled with energy dispersive X-ray spectroscopy (EDXS) mapping of metals on the catalyst. Also, to investigate the reducibility of metal oxide into metals H_2-temperature programmed reducibility tests were performed using a Schimadzu TGA-50 with a hydrogen atmosphere.

3. RESULTS AND DISCUSSION.

3.1. Two stage (i) pyrolysis (ii) catalytic steam reforming

The initial investigation concerned identifying the optimum conditions for the first two stages of the three stage system involving only (i) pyrolysis (ii) catalytic steam reforming to maximize the output of carbon oxides (and hydrogen) for catalytic hydrogenation in the third stage catalytic hydrogenation reactor. The influence of pyrolysis temperature on the product yield and pyrolysis gas composition from the pyrolysis of the same biomass wood sawdust used in this work was presented in our previous article [19]. However, these results may be summarised as, with the increase in the final pyrolysis temperature from 500 to 800 °C, the amount of residual char decreased, showing that the biomass continued to thermally decompose at higher pyrolysis temperatures. The increased biomass degradation resulted in an increase in the yield of product liquid and a smaller increase in product gas yield. The increased gas yield reflecting an increase in CH_4, H_2, CO, and CO_2 yield as the final pyrolysis

temperature was raised from 500 to 800 °C. Therefore, for the current study the biomass pyrolysis was carried out at the optimized higher final pyrolysis temperature of 800°C. The influence of the catalytic steam reforming temperature and influence of the input steam WHSV were carried out using the 1st stage pyrolysis and 2nd stage steam reforming reactor system, with the third stage catalytic hydrogenation reactor removed. The catalyst used for these experiments was 10 wt. % Ni/Al_2O_3.

3.1.1. Influence of catalyst steam reforming temperature

The influence of the catalytic steam reforming temperature on the product yield and the gas composition was carried out at temperatures of range of 600 °C,700 °C,800 °C and900 °C. The biomass was pyrolysed under the temperature regime of ambient temperature to 800 °C at a heating rate of 20 °C min^{-1}[19]. The catalyst used was 10 wt.% Ni/Al_2O_3 with an input steam WHSV of 3 mL h^{-1} $g^{-1}_{catalyst}$. Table 2 shows the product yield, gas ratios and volumetric gas composition (vol.%). In addition, Figure 2 shows the gas yield in mmoles $g^{-1}_{biomass}$.

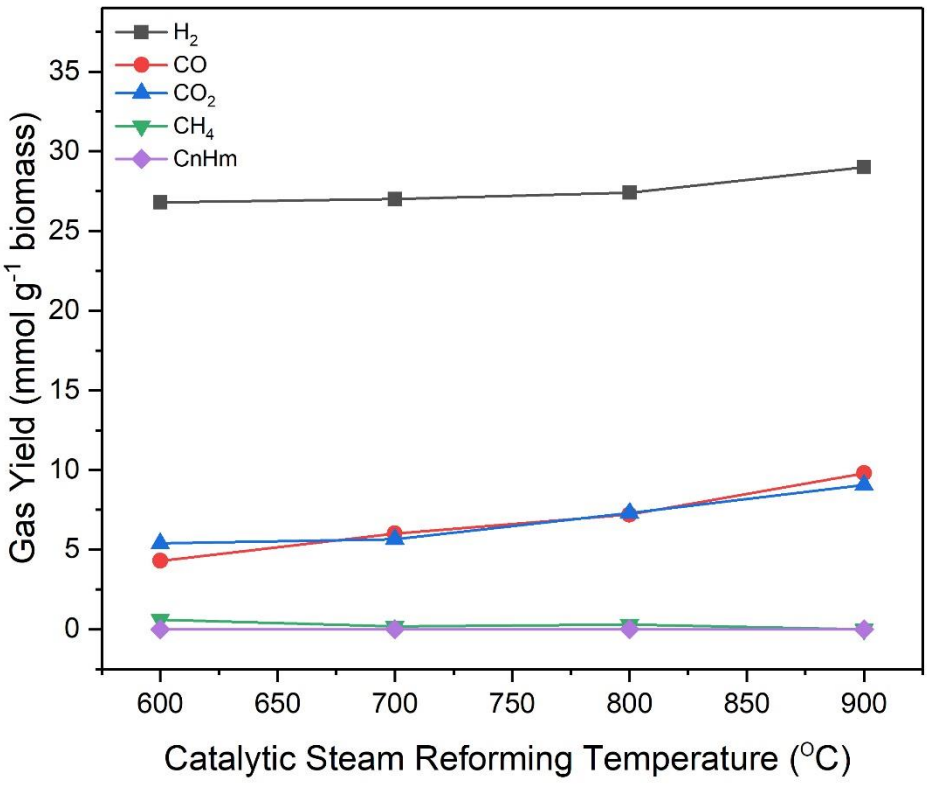

Figure 2 Influence of catalytic steam reforming temperature on gas yield (pyrolysis temperature 800 °C, Steam WHSV3 mL h^{-1} $g^{-1}_{catalyst}$).

The results suggest that with the increase in the catalytic steam reforming temperature from 600 to 900 °C the overall gas yield increased from 42.5 to 73.4 wt.%, with a consequent decrease in liquid yield from 37.43 to 6.6 wt. %. The liquid was mostly composed of water. Since, the 1st stage pyrolysis temperature conditions remained the same for each experiment, the solid char yield remained constant at ~20 wt. %. Table 2 also shows the distribution of carbon in the gas, and solid products. The carbon distribution in the char was the same for each experiment at 33.53 %. It can be seen from Table 2 that with the increase in catalytic reforming temperature percentage of carbon in the gaseous product increased from 25.12 to 45.45 %. The distribution of carbon in the liquid products was not calculated because only a

trace of bio-oil was present in the liquid product water and it was not possible to separate using methods such as Karl-Fischer titration. For comparison a blank experiment was performed using quartz sand in place of the 10 wt.% Ni/Al_2O_3 catalyst. The sand representing a hot bed of particulate material, but with no catalyst metal present. It was observed that in the presence of sand the liquid yield was higher and gas yield was lowered as compared to when a catalyst was present. This suggests that the catalyst reforming reaction was promoted over the active metal sites of the catalyst compared to that of sand, where mostly thermal cracking with some steam reforming would occur.

Figure 2 also shows that with the increase in catalytic steam reforming temperature from 600 to 900 °C the H_2, CO, and CO_2 yields showed a continuous increase. The H_2 yield increased from 26.8 to 28.94 mmoles $g^{-1}_{biomass}$ together with an increase in CO yield from 4.36 to 9.83 mmoles $g^{-1}_{biomass}$ and CO_2 yield from 5.41 to 9.06mmoles $g^{-1}_{biomass}$. The increase in H_2 and CO_2 yield with the decrease in liquid yield and CH_4/CO_2 gas ratio was due to cracking and reforming reactions (eqs. 2-6). It was also observed that the H_2/CO ratio was decreased and CO/CO_2 ratio was increased with the increase in catalyst temperature because of the reverse water gas shift reaction (eq 7). It has been reported by many researchers that the water gas shift reaction is favourable at lower temperatures, however, at higher temperatures, equilibrium shift takes place and results in the promotion of the reverse water gas shift reaction [20, 21]. Another possible reason for the increase in CO/CO_2 ratio was the Boudouard reaction (eq 8) which is favourable at higher temperature ranges [22]. Luo et al., [23] investigated the effect of catalytic steam reforming temperature in the temperature range of 600 to 900 °C for the production of hydrogen from biomass (palm sawdust). Calcined dolomite was used as the catalyst with a steam to biomass ratio of 1.2. It was observed that with the increase in temperature from 600 to 900 °C, H_2 yield increased from 2.02 to 25.38 mmoles $g^{-1}_{biomass}$. Gao et al., [24] used pine sawdust as the biomass feedstock in a fixed bed

283 reactor to investigate the effect of reforming temperature in the range of 800 to 950 °C on
284 hydrogen yield. Catalytic steam reforming was carried out over porous ceramic material and
285 the steam/biomass ratio was kept constant at 1.4. It was observed that with the increase in
286 reactor temperature from 800 to 950 °C, the H_2 yield increased from 24.98 to 39.95 mmoles
287 $g^{-1}_{biomass}$. They suggested that the increase in H_2 yield was due to the promotion of thermal
288 cracking and steam reforming reactions. Similarly, Waheed et al., [25] investigated different
289 biomass feedstocks i.e. rice husk, sugar cane bagasse, and wheat straw for H_2 production in a
290 two-stage fixed bed reactor using 10 wt.% Ni/dolomite as catalyst. Catalytic bed temperature
291 was at 950 °C and steam/biomass ratio was 1.37. The H_2 yield obtained over rice husk, sugar
292 cane bagasse, and wheat straw were 23.71, 21.18 and 21.59 mmoles $g^{-1}_{biomass}$ respectively.
293 Akubo et al., [26] also used a similar two-stage pyrolysis-catalytic steam reforming reactor to
294 investigate different biomass feedstocks for hydrogen production. The biomass feedstocks
295 used were rice husk, coconut shell, sugar cane, palm kernel shell, cotton stalk, and wheat
296 straw. The catalyst used was 10 wt.% Ni/Al_2O_3 at a reforming temperature of 750 °C with a
297 steam WHSV of 5.7 mL h^{-1} $g^{-1}_{catalyst}$. They reported that rice husk, coconut shell, sugar cane,
298 palm kernel shell, cotton stalk, and wheat straw produced 18.22, 22.11, 22.96, 25.35, 20.74
299 and 16.38 mmoles H_2 $g^{-1}_{biomass}$ respectively. From the current study, it may be concluded that
300 high temperatures are favourable for converting the higher molecular weight hydrocarbons
301 into lower molecular weight gaseous products.
302
303 **3.1.2. Influence of steam weight hourly space velocity (WHSV).**
304
305 The influence of input steam WHSV on the product yield from (i) biomass pyrolysis and (ii)
306 catalytic steam reforming was carried out in the range of 1 to 9 mL h^{-1} $g^{-1}_{catalyst}$. The catalyst
307 used was 10 wt.% Ni/Al_2O_3 and catalytic steam reforming temperature were maintained at

800 °C. Product yield, gas ratios and volumetric gas composition (vol.%) are shown in Table 3. Also Table 3 shows the percentage carbon in the product gas. Figure 3 shows the gas yield in relation to the mass of biomass (mmoles $g^{-1}_{biomass}$).

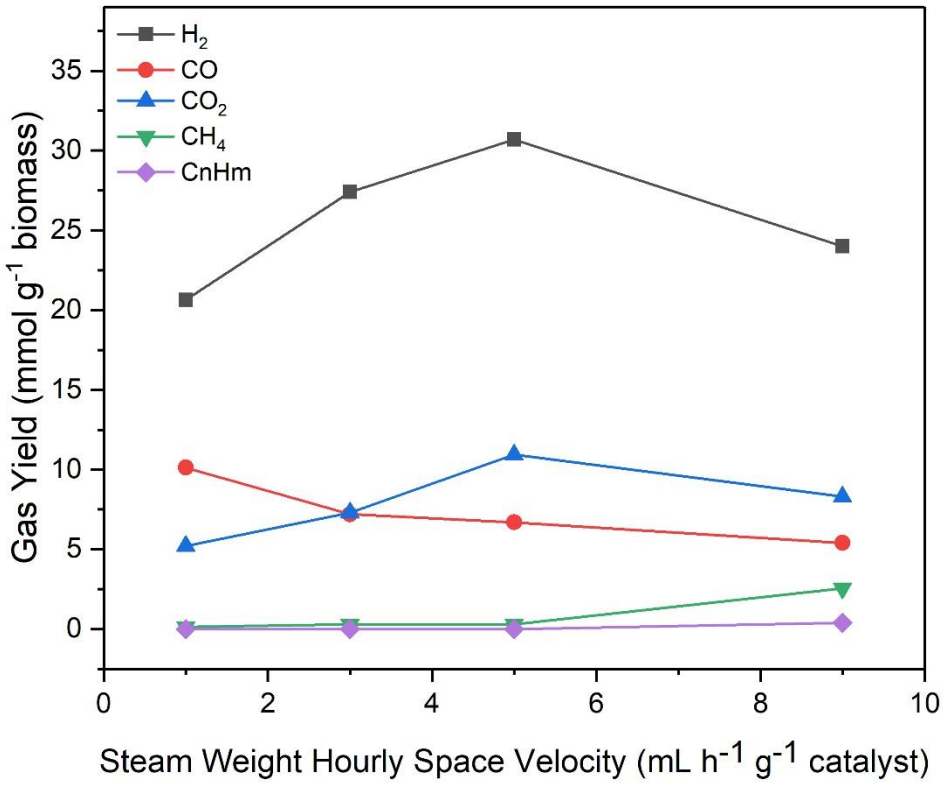

Figure 3 Influence of steam WHSVon the gas yield (pyrolysis temperature 800 °C, Catalytic steam reforming temperature 800 °C).

Table 3 includes the comparison between the sand and the catalyst at the steam WHSV of 3 mL h^{-1} $g^{-1}_{catalyst}$, the total gas yield increased from 44.83 to 58.5 wt.% when the sand was replaced by the catalyst, suggesting addition of catalyst promoted the catalytic steam reforming and reforming reactions (eqs. 2 – 6). With the increase in steam WHSV from 1 to 5 mL h^{-1} $g^{-1}_{catalyst}$, it was observed that the gas yield increased from 55.7 to 73.85 wt.%. However, with the further increase in steam WHSV to 9 mL h^{-1} $g^{-1}_{catalyst}$ the gas yield reduced

to 60.48 wt.%. The solid char remained at ~20 wt.% because the pyrolysis stage temperature conditions were the same for each experiment. It can be seen from Table 3 that with the increase in steam WHSV from 1 to 5 mL h^{-1} $g^{-1}_{catalyst}$, the percentage carbon in the gaseous product increased from 35.34 to 43.41wt.%. However with the further increase in steam WHSV to 9 mL h^{-1} $g^{-1}_{catalyst}$ the percentage carbon in the gas decreased to 41.04 wt.%. It may be suggested that an optimum steam WHSV enhances the catalytic tar conversion into low molecular weight gaseous products and results in the increase of carbon content in the gaseous output product. However at higher steam WHSV, catalytic hydrocarbon conversion into low molecular weight gaseous product was reduced therefore resulting in the reduced carbon content in the gaseous product. The influence of the steam/biomass (S/B) ratio on carbon conversion has also been reported by Franco et al., [27]. Carbon conversion was calculated based on the carbon content in the gaseous product in relation to the carbon content in the feedstock. Gasification of pine waste was carried out in a bench scale fluidized bed reactor. They reported that with the increase in S/B ratio the gaseous product yield along with carbon conversion initially increased, which corresponded to the minimum liquid yield. However, with a further increase in the S/B ration, the carbon conversion was reduced. Similarly, Quan et al., [28] investigated the influence of S/B ratio on the reforming of bio-oil in a fixed bed reactor. They also reported that with the initial increase in S/B ratio up to the optimal ratio, had a positive effect on carbon conversion into gas. This was due to the promotion of the water gas shift reaction and reforming reaction. But the increase in S/B ratio higher than the optimal ratio resulted in a reduction in carbon conversion into gas product due to the suppression of the reforming reaction.

Figure 3 shows that with the increase in steam WHSV from 1 to 5 mL h^{-1} $g^{-1}_{catalyst}$, H_2 and CO_2 yields increased with a corresponding decrease in CH_4 and CnHm yields, due to

steam reforming reactions (Eqs. 3-6). However with the further increase in steam WHSV to 9 mL h^{-1} $g^{-1}_{catalyst,}$ H_2, CO and CO_2 yield reduced while CH_4 and CnHm yield increased. The highest H_2, and CO_2 yield of 30.68, and 10.93 mmoles $g^{-1}_{biomass}$ was obtained at the steam WHSV of 5 mL h^{-1} $g^{-1}_{catalyst}$. The increase in the H_2, and CO_2 along with the decrease in CH_4/CO_2 and CH_4/CO ratio was associated with the promotion of cracking and reforming reactions with the increase in steam WHSV up to 5 mL h^{-1} $g^{-1}_{catalyst}$, however with the further increase in steam WHSV to 9 mL h^{-1} $g^{-1}_{catalyst}$, cracking and reforming reactions were suppressed and resulted in the formation lower H_2, and CO_2 yield. As can be seen from Table 3 the H_2/CO ratio increased and CO/CO_2 ratio decreased with the increase in steam WHSV from 1 to 5 mL h^{-1} $g^{-1}_{catalyst}$ showing the promotion of the water gas shift reaction (eq 7). Similar results have been reported by Li et al., [29] when they carried out the steam gasification of biomass palm-oil waste in a bench scale combined fixed bed reactor at 900 °C catalyst bed temperature. They reported that with the increase in steam WHSV from 0 to 0.6 mL h^{-1} $g^{-1}_{catalyst}$ the H_2 yield increased from 25.11 to 61.5 mmoles $g^{-1}_{biomass}$. However, with the further increase in steam WHSV to 0.8 mL h^{-1} $g^{-1}_{catalyst}$ H_2 yield reduced to 58.05 mmoles $g^{-1}_{biomass}$. They suggested that the initial increase in hydrogen yield was because of the water gas and water gas shift reactions while the decrease in the hydrogen yield was observed because of the decrease in reaction temperature due to excess steam flowing through the reactor system.

3.2. Three stage (i) pyrolysis (ii) catalytic steam reforming (iii) catalytic hydrogenation

The third stage catalytic hydrogenation reactor was added to the two-stage reactor configuration to produce the three stage (i) pyrolysis (ii) catalytic steam reforming (iii) catalytic hydrogenation reactor system (Figure 1). The following sections report on the

influence of various process parameters particularly targeted at the reactions of the 3rd stage catalytic hydrogenation process. Consequently, the (i) pyrolysis process parameters and the (ii) catalytic steam reforming process parameters were kept constant for this series of experiments; the biomass pyrolysis temperature programme was ambient temperature to 800 °C at a heating rate of 20 °C min^{-1}; catalytic steam reforming involving,10 wt.% Ni/Al_2O_3 catalyst held at 800 °C and input steam at a WHSV of 5 mL h^{-1} $g^{-1}_{catalyst}$. The catalyst used in the catalytic hydrogenation reactor was 10 wt.% Ni/Al_2O_3 because of its higher catalytic activity and selectivity towards the methanation reaction [30].

3.2.1. Influence of catalytic hydrogenation temperature

The influence of the 3rd stage catalytic hydrogenation reactor temperature was investigated in the temperature range of 250°C, 300 °C, 350 °C and 400 °C and the results for product yield, gas ratios and volumetric gas composition (vol.%) are shown in Table 4. Hydrogen gas with a space velocity of 3600 mL h^{-1} $g^{-1}_{catalyst}$ was introduced into the 3rd stage catalytic hydrogenation reactor [19]. Figure 4 shows the gas yield in relation to the mass of biomass in mmoles $g^{-1}_{biomass}$.

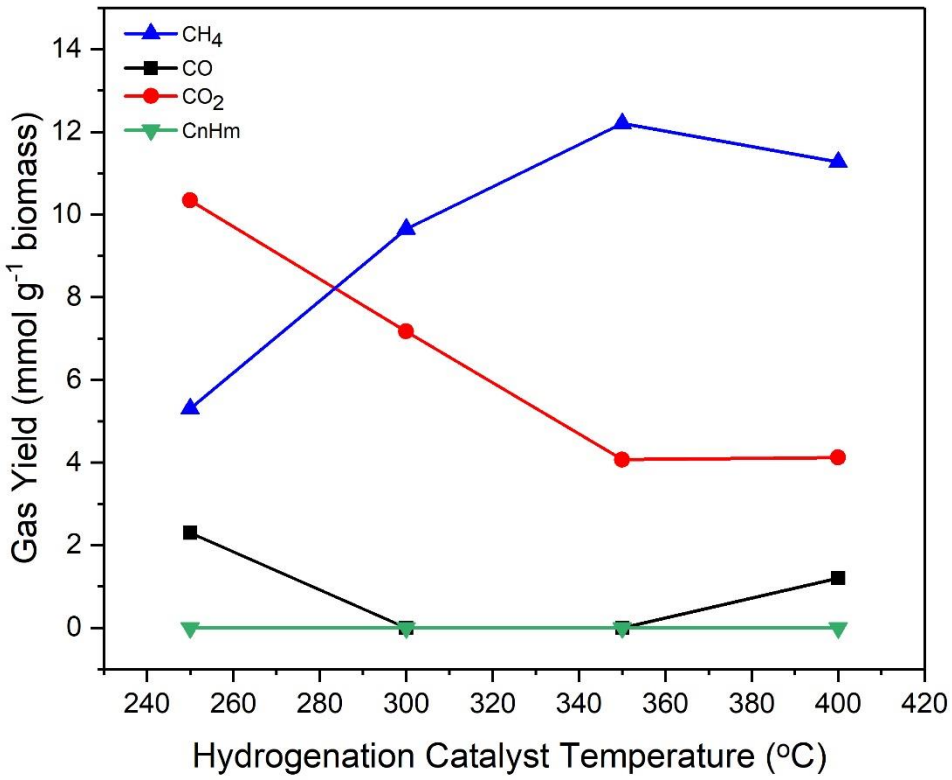

Figure 4 Influence of catalytic hydrogenation temperature on the gas yield (Pyrolysis temperature 800 °C, Catalytic steam reforming temperature 800 °C, Steam WHSV5 mL h^{-1} $g^{-1}_{catalyst}$).

The gas composition (vol.%) shown in Table 4 shows that the gas product produced from the three-stage process produces a gas with a high volumetric composition of methane, the highest being 75 vol.% methane with 25 vol.% carbon dioxide at a catalytic hydrogenation temperature of 350 °C. The total gas yield including the gas produced from the biomass as well as added hydrogen decreased from 96.78 to 66.98 wt.% with the increase in hydrogenation catalyst temperature. Suggesting that at lower temperature, most of the hydrogen gas passed over the catalyst bed unreacted, which resulted in the increase in the total gas yield. It was not possible to calculate liquid yield produced from the biomass because of the addition of steam in the catalytic steam reforming stage of the reactor system.

403 But, liquid water produced as the result of the methanation reaction increased from 12 wt.%
404 to 39 wt.% with the increase in catalytic hydrogenation temperature which showed the
405 promotion of the methanation reactions (Eqs. 10-11). Table 4 shows that the percentage
406 carbon content in the product gases remained roughly the same at all the catalytic
407 hydrogenation temperatures studied because the carbon from gaseous CO_2 and CO was
408 converted into gaseous CH_4. Also, the carbon contribution in the char remained at 33.53 wt.%
409 for all the experimental conditions, because of the fixed biomass pyrolysis temperature
410 conditions.

411 Figure 4 shows that the methane yield increased from 5.30 to 12.18 mmoles $g^{-1}_{biomass}$
412 with the increase in catalytic hydrogenation temperature from 250 to 350 °C. Also, CO yield
413 reduced from 2.39 to 0.0 mmoles $g^{-1}_{biomass}$ while CO_2 yield reduced from 10.34 to 4.07
414 mmoles $g^{-1}_{biomass}$. However, with the further increase in hydrogenation catalyst temperature to
415 400 °C, CH_4 yield reduced to 11.27 mmoles $g^{-1}_{biomass}$ along with the formation of some CO at
416 1.204 mmoles $g^{-1}_{biomass}$ while the CO_2 yield slightly increased to 4.12 mmoles $g^{-1}_{biomass}$. The
417 reason for the initial increase in CH_4 yield and decrease in CO and CO_2 yields up to 350 °C
418 was the promotion of the methanation reactions of CO and CO_2 (Eqs. 10 – 11). Table 4
419 shows that the CH_4/CO_2 ratio increased from 0.51 to 2.99 while CO was completely
420 converted to methane at a catalyst temperature of 350 °C. While at 400 °C some CO was
421 detected and the CH_4/CO_2 ratio was reduced to 2.73 showing the decline in the methanation
422 reaction. The increase in CO yield at 400 °C was due to the promotion of the reverse water
423 gas shift reaction which is enhanced at elevated temperatures. Lu et al., [31] investigated CO
424 methanation with a Ni-ZrO_2 catalyst. They also showed that CO methanation takes place at
425 lower temperature compared to CO_2 methanation. They observed the maximum CO
426 conversion at 350 °C but the methane selectivity was reduced when the catalyst temperature
427 was increased from 350 to 500 °C. Also, Rahmani et al., [32] carried out CO_2 methanation

428 over a nickel-alumina catalyst. They reported that the highest methane yield was observed at
429 350 °C due to the promotion of the methanation reaction but, CH_4 yield started reducing at
430 400 °C because of the decomposition of CO_2 into other side products. According to Zhang et
431 al., [33], the decrease of CO_2 conversion to CH_4 at high temperatures was because of the
432 promotion of the reverse water gas shift reaction at elevated temperature. The current study
433 suggests that the optimum hydrogenation temperature of 350 °C is required to maximise
434 carbon oxides conversion to methane.
435
436 **3.2.2. Influence of H_2 space velocity for catalytic hydrogenation**
437
438 The influence of the amount of added hydrogen into the 3rd stage catalytic hydrogenation
439 reactor in terms of hydrogen space velocity was studied in the range of 0 to 3600 mL h^{-1} $g^{-1}_{catalyst}$. The catalyst used in the catalytic hydrogenation reactor was 10 wt.% Ni/Al_2O_3 at a
441 catalytic hydrogenation temperature of 350 °C. Table 5 shows the results in terms of
442 hydrogen space velocity in relation to the product yield, gas ratios and volumetric gas
443 composition. Figure 5 shows the gas yield in relation to the mass of biomass feedstock in
444 mmoles $g^{-1}_{biomass}$.

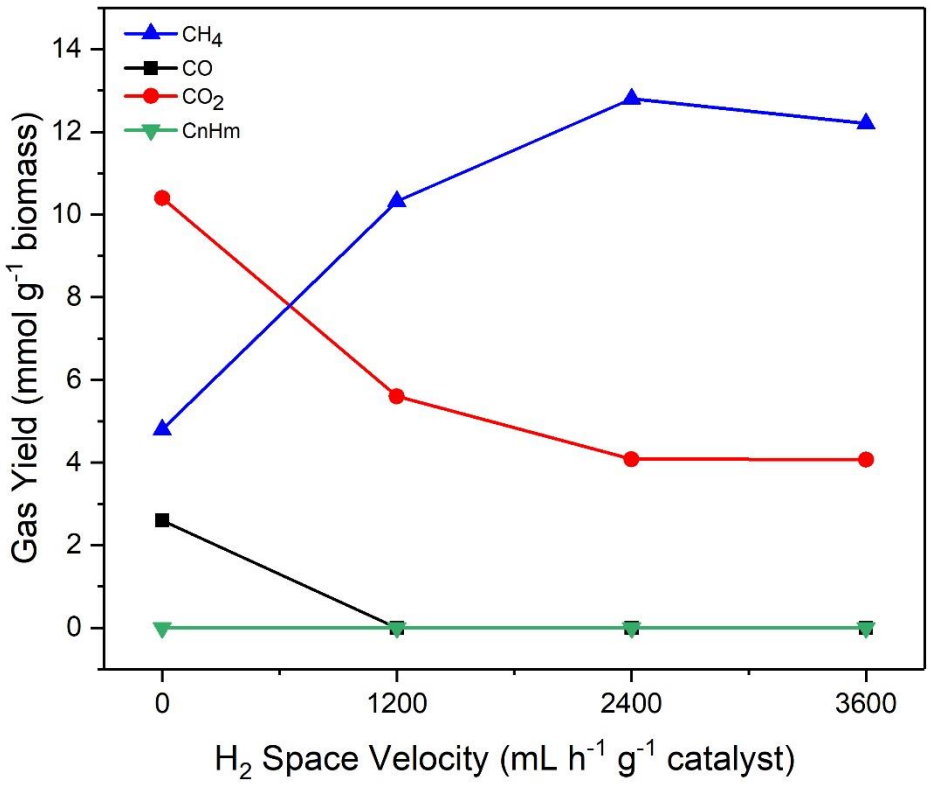

Figure 5 Influence of hydrogen space velocity on the gas yield (Pyrolysis temperature 800 °C, Catalytic steam reforming temperature 800 °C, Steam WHSV5 mL h^{-1} $g^{-1}_{catalyst}$, Catalytic hydrogenation temperature 350 °C).

Table 5 shows that the gas yield produced from biomass and added hydrogen increased from 60.78 to 67.95 wt. % with the increase in H_2 space velocity from 0 to 3600 mL h^{-1} $g^{-1}_{catalyst}$. Also, a significant increase in water yield derived from the methanation reactions was observed, rising from 12 to 39 wt.% with the increase in H_2 space velocity from 0 to 2400 mL h^{-1} $g^{-1}_{catalyst}$ which showed the enhancement of methanation reactions. Water produced as the result of methanation reaction decreased to 37 wt.% with the further increase in H_2 space velocity to 3600 mL h^{-1} $g^{-1}_{catalyst}$. Table 5 also shows the carbon percentage in the solid, and gaseous products. The percentage carbon content in the char remained the same i.e. 33.53 wt.% at all the H_2 space velocity investigated because the final pyrolysis temperature in all the experiments was fixed at 800 °C. But at the lower hydrogen space velocities, carbon

459 deposition over the catalyst was observed which resulted in a slight increase of carbon
460 content in the solid product to 33.609 and 33.569 at the space velocities of 0 and 1200 mL h^{-1}
461 $g^{-1}_{catalyst}$ respectively. However, the percentage carbon in the gaseous products obtained at
462 different H_2 space velocities did not show any significant difference. The carbon content of
463 the liquid bio-oil was not possible to analyse because of the collection of a significant amount
464 of unreacted steam condensate in the condenser. Table 5 shows that with the increase in
465 hydrogen space velocity to the higher input hydrogen rates of 2400 and 3600 mL h^{-1} $g^{-1}_{catalyst}$
466 the product CH_4 volumetric gas concentration increased to ~75 vol.% with the only other gas
467 being CO_2. This showed the promotion of methanation reactions when the hydrogen space
468 velocity was increased to the higher hydrogen inputs.

469 Figure 5 shows that with the increase in hydrogen space velocity from 0 to 2400 mL
470 h^{-1} $g^{-1}_{catalyst}$, methane yield increased significantly from 4.78 to 12.77 mmoles $g^{-1}_{biomass}$. The
471 CO_2 yield was reduced from 10.41 to 4.02 mmoles $g^{-1}_{biomass}$ and CO yield reduced to 4.7 to
472 0.0 mmoles $g^{-1}_{biomass}$. With the further increase in hydrogen space velocity to 3600 mL h^{-1} $g^{-1}_{catalyst}$, methane yield was reduced slightly with a similar slight increase in CO_2 yield. This
474 increase in methane yield together with the decrease in CO and CO_2 at higher hydrogen space
475 velocities was because of the promotion of the methanation reaction (Eqs. 10-11). It is also
476 evident from Table 5 that with the increase in hydrogen space velocity, the CH_4/CO_2 ratio
477 increased from 0.45 to 3.17 and the complete conversion of CO was achieved with the
478 increase in hydrogen space velocity from 0 to 2400 mL h^{-1} $g^{-1}_{catalyst}$. While with the further
479 increase in hydrogen space velocity to 3600 mL h^{-1} $g^{-1}_{catalyst}$ the CH_4/CO_2 ratio decreased to
480 2.99, because the higher space velocity results in the lower conversion of reactant gases over
481 the catalyst because of shorter residence time. In addition, an optimum H_2:COx ratio is
482 required to carry out the methanation reaction. Li et al., [34] studied the effect of space
483 velocity of reactant syngas (H_2 and CO) on the methanation reaction over a nickel-alumina

484 catalyst in the range of 5000-40,000 h^{-1}. There was a negligible difference observed on CO
485 conversion and methane selectivity when high space velocities of 5000 h^{-1} and 10,000 h^{-1} was
486 employed. However, with the increase in space velocity from 10,000-40,000 h^{-1} CO
487 conversion reduced significantly because of the shorter contact time between the catalyst and
488 reactant gases. Similarly, Pastor-Pérezet al., [35] reported results on the influence of reactant
489 gas space velocity using H_2/CO_2 with a ratio of 4:1 balanced in nitrogen in relation to CO_2
490 conversion in the range of 6250 - 25000 mL h^{-1} $g^{-1}_{catalyst}$ using a Ni-Co/Ce-Zr catalyst. They
491 also, reported that the decrease in CO_2 conversion at higher space velocity and these results
492 were more significant at higher temperatures. Kang et al., [36] and Aziz et al., [15] showed
493 that maximum CO and CO_2 conversion is achievable at the stoichiometric ratio. According to
494 them, COx conversion was reduced when the H_2/CO and H_2/CO_2 ratios were increased above
495 the stoichiometric ratios. However, some research has reported that the H_2:COx ratio
496 equivalent to, or higher than the stoichiometric ratios are both favourable for methanation
497 reaction. However, below the stoichiometric ratio, carbon deposition on the catalyst resulting
498 in lower catalytic activity and selectivity was observed [37, 38]. Therefore, these results
499 suggest that an optimal hydrogen space velocity is required to enhance the carbon oxides
500 methanation reaction. Our research suggests that for the reactor system used here, the highest
501 methane yield was obtained at the higher hydrogen space velocities of 2400 -3600 mL h^{-1} $g^{-1}_{catalyst}$.
502
503

3.3. Optimisation of the stage three hydrogenation catalyst

A further investigation into the optimisation of the three stage pyrolysis-catalytic steam reforming-catalytic methanation reaction process involved the development of the catalyst used in the third stage methanation reactor. The catalyst parameters investigated were the influence of different catalyst active metals, influence of catalyst calcination temperature, different catalyst metal loadings and different catalyst support materials. The experiments were carried out with the optimised process conditions from the previous sections. That is, pyrolysis of biomass via a heating rate of 20 °C min^{-1} to the final pyrolysis temperature of 800 °C, catalytic steam reforming temperature of 800 °C with the 10 wt.% Ni/Al_2O_3 catalyst, steam input to the reforming reactor of WHSV 5 mL h^{-1} $g^{-1}_{catalyst}$, third stage catalytic hydrogenation temperature of 350 °C, and input hydrogen space velocity 2400 mL h^{-1} $g^{-1}_{catalyst}$.

3.3.1. Influence of metal-Al_2O_3 catalyst type for catalytic hydrogenation

The influence of the type of metal-alumina catalyst in relation to the production of methane from the catalytic hydrogenation of biomass using the three stage (i) pyrolysis (ii) catalytic steam reforming (iii) catalytic hydrogenation reactor system was investigated. The different metals investigated were Fe, Co, Mo and Ni at 10 wt.% metal concentration i.e., 10 wt.% Fe/Al_2O_3, 10 wt.% Co/Al_2O_3, 10 wt.% Mo/Al_2O_3, and 10 wt.% Ni/Al_2O_3 catalysts. The catalytic hydrogenation reactor was maintained at 350 °C with a hydrogen space velocity of 2400 mL h^{-1} $g^{-1}_{catalyst}$. The results are shown in Table 6 in terms of the influence of different metal-alumina catalysts in relation to product yield, gas ratios and volumetric gas composition. Table 6 also shows the results produced where sand was used in place of the

529 metal-alumina catalysts. Figure 6 shows the gas yield results in terms of mmoles $g^{-1}_{biomass}$. It
530 can be seen from Table 6 that the highest CH_4/CO_2 ratio was obtained with the 10 wt.%
531 Ni/Al_2O_3 catalyst and almost all of the CO was converted into methane which illustrates the
532 effective catalytic activity and selectivity for methane production. The cobalt based catalyst
533 (10 wt.% Co/Al_2O_3) showed good catalytic activity and selectivity for methane and resulted
534 in high CH_4/CO and CH_4/CO_2 ratios of 7.6 and 2.3 respectively. It can also be seen from
535 Table 6 that the catalysts which showed the lowest methanation activity resulted in the
536 highest gas yield with low methanation water formation because most of the H_2 gas and the
537 output product gaseous mixture derived from the 2^{nd} stage reforming reaction passed over the
538 catalyst bed unreacted. Similarly, the nickel catalyst showed the highest yield of water
539 produced as a result of methanation reactions. Table 6 also shows the percentage carbon in
540 the gaseous product. There was no significant difference observed in the carbon content of
541 the gaseous products for the different catalysts investigated.

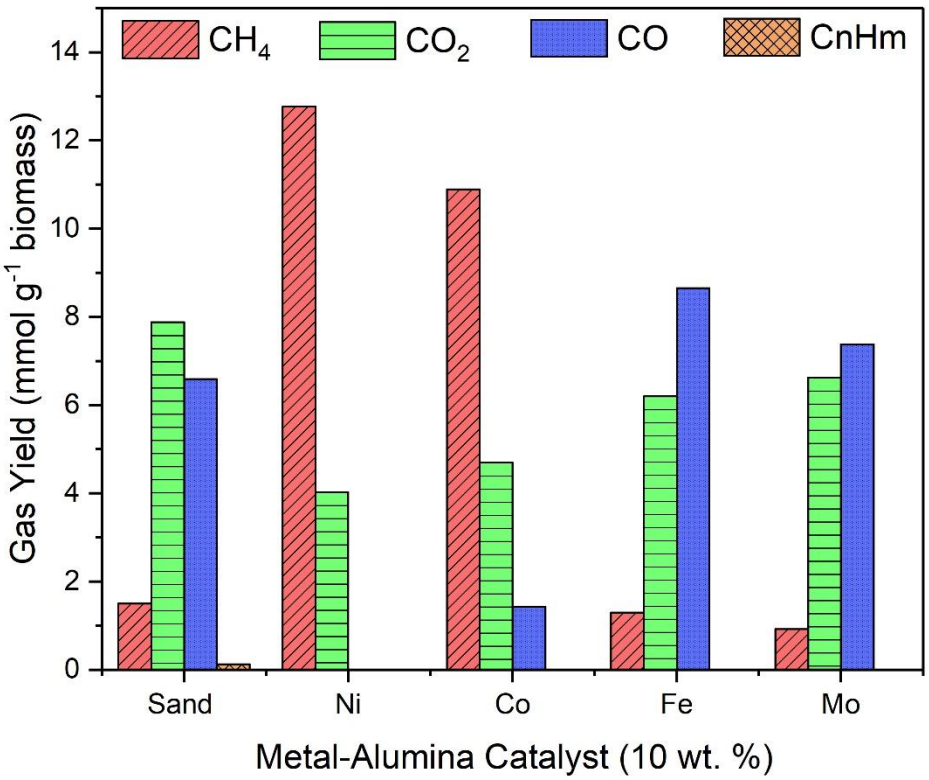

Figure 6 Influence of 10 wt. % metal- alumina catalysts on gas yield (pyrolysis temperature 800 °C, Catalytic steam reforming temperature 800 °C, Steam WHSV5 mL h^{-1} $g^{-1}_{catalyst}$, Catalytic hydrogenation temperature 350 °C, and Hydrogen space velocity 2400 mL h^{-1} $g^{-1}_{catalyst}$).

The highest volumetric gas composition for methane gas was 76.0 vol.% (Table 6) obtained over the Ni/Al_2O_3 catalyst followed by Co/Al_2O_3 catalyst at 64.0 vol.% methane. However catalytic activity and selectivity for methane production with the Fe/Al_2O_3 and Mo/Al_2O_3 catalysts was significantly lower producing a product gas composition with low methane content and high CO_2 and CO content comparable to that of the baseline sand experiments.

It can be seen from Figure 6 that the highest methane yield in terms of the mass of biomass was obtained over the Ni/Al_2O_3 catalyst at 12.77 mmoles $g^{-1}_{biomass}$ followed by the

556 Co/Al_2O_3 catalyst at 10.89 mmoles $g^{-1}_{biomass}$. However, the Fe and Mo based catalysts
557 (Fe/Al_2O_3 and Mo/Al_2O_3) showed very low selectivity for methane production. The catalytic
558 activity in relation to methane production in terms of the metal-alumina catalysts was in the
559 following order Ni > Co > Sand > Fe > Mo.

560 Fischer et al., [39] investigated the methanation reaction in relation to the catalytic
561 activity of various metals and reported that the methanation activity increased in the order;
562 Ag < Pd < Mo < Fe < Pt < Os < Co < Ni < Rh < Ru. A similar trend of catalytic activities of
563 the investigated catalysts were observed in the current study. It is evident from Figure 6 that
564 the catalytic activity of Fe and Mo based catalysts resulted in higher CO yield with some CO_2
565 conversion as compared to the baseline sand. While a negligible change in the CH_4 yield was
566 observed. This suggested that the Fe and Mo based catalysts promoted the reverse water gas
567 shift reaction instead of methanation reactions. The high water gas shift activity of Fe and Mo
568 based catalysts has been reported by other researchers [40, 41]. Similarly, when the catalytic
569 activity of Ni and Co based catalysts were compared with the baseline sand, the higher yield
570 of CH_4 was observed with the lower yields of CO and CO_2 which reflects the promotion of
571 methanation reactions.

572

573 Other researchers have reported on the influence of different types of metal based
574 catalysts in relation to carbon monoxide methanation. Konshcheva et al., [42]carried out CO
575 methanation using Ni, Fe and Co metal catalyst loaded on CeO_2 support. They also reported a
576 higher catalytic activity for the nickel based catalyst for methane production compared to the
577 cobalt based catalyst. They also reported that the Fe/CeO_2 catalyst remained inactive during
578 CO methanation. Takenaka et al., [43] carried out an investigation of different metal/SiO_2
579 catalysts. They also reported the poor activity of the Fe metal based catalyst compared to that
580 of Ni and Co. Hu et al., [44] studied the effect of Mo-carbide and Co-Mo/carbide for CO

methanation. They reported that molybdenum alone showed lower catalytic activity compared to that when used as a promotor in Co-Mo/carbide catalyst.

The methanation of carbon dioxide has also been investigated by several researchers. Aziz et al., [45] studied the methanation of CO_2 with different metal-based catalysts (Ni, Fe, Rh, Ru, Ir, Cu) loaded on SiO_2 support. They reported that the activity of the metal-SiO_2 catalysts was dependant on the reaction temperature. The highest catalytic activity was reported over the nickel based catalyst in the temperature range of 473 to 673 K. Similarly, Alrafei et al., [46] studied the comparison of nickel and cobalt based metal catalysts. They reported the high selectivity and activity of the cobalt catalyst, but, the Co based catalyst showed lower catalytic activity in terms of carbon dioxide conversion compared to that of the nickel based catalyst. Some researchers have also focussed on the use of Fe, Co, Mo as second promoter metals to enhance the catalytic activity of nickel [47-49]. It has been reported that the presence of the second metal improves the catalyst stability towards sintering and results in a synergetic effect which enhances the catalytic activity.

3.3.2. Influence of catalyst calcination temperature for catalytic hydrogenation

The influence of catalyst calcination temperature used in the preparation process of the 10 wt.% Ni/Al_2O_3 catalyst was also investigated to determine the influence on methane production from biomass using the three stage (i) pyrolysis (ii) catalytic steam reforming (iii) catalytic hydrogenation reactor system. Our previous work has shown that the calcination temperature used for catalyst preparation strongly influences the physical properties of surface area and porosity on the resultant catalysts and thereby also influences the production of methane from biomass during the catalytic hydrogenation process [19]. The catalyst calcination temperatures investigated in this work were 650, 750, 850 and 950 °C.

606 The prepared catalysts were characterized by using hydrogen-temperature
607 programmed reduction (H_2-TPR) via a thermogravimetric analyser to investigate the
608 reducibility of nickel oxide into metallic nickel. The results of the H_2-TPR analysis are shown
609 in Figure 7. The TGA-TPR thermograms showed that the catalyst calcined at a calcination
610 temperature of 650 °C showed the highest weight loss followed by those calcined at 750, 850
611 and 950 °C. The catalyst calcined at 950 °C showed the highest stability and minimum
612 weight loss. More weight loss was observed for the catalysts calcined at lower calcination
613 temperatures because the NiO particles are uniformly distributed over the support. It has been
614 suggested that the support acts as the dispersion media at lower calcination temperature and is
615 therefore prone to easier reduction to metallic Ni and thereby results in the formation of H_2O.
616 But at higher calcination temperature, Al_2O_3 reacts with NiO and results in the formation of a
617 solid solution which decreases the reducibility and enhances the catalyst stability [50]. It can
618 therefore be concluded, that with the increase in catalyst preparation calcination temperature,
619 the interaction between metal and support becomes stronger and results in higher catalyst
620 stability. These results are in good agreement with the results observed by Aljishi et al., [51].
621 They carried out H_2-TPR analysis of a nickel alumina catalyst. They also reported that with
622 the increase in catalyst calcination temperature the interaction between the nickel and
623 alumina support increases.

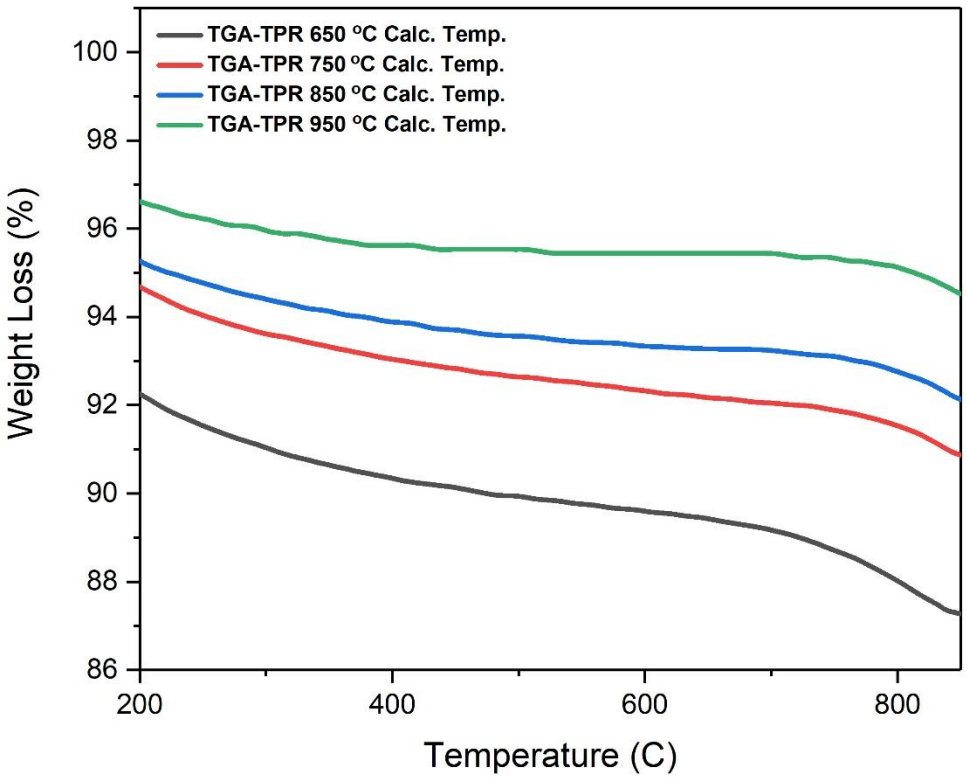

624

625 **Figure 7** H_2 TGA-TPR of 10 wt. % Ni/Al_2O_3 catalysts calcined at various temperatures

626

627 The 10 wt.% Ni/Al_2O_3 catalysts calcined at different calcination temperatures were
628 used in the catalytic hydrogenation reactor to determine the influence on methane production.
629 The catalytic hydrogenation reactor temperature was fixed at 350 °C with hydrogen space
630 velocity of 2400 mL h^{-1} $g^{-1}_{catalyst}$. The reaction conditions in the 1st and 2nd stage reactors were
631 maintained as before. Table 7 shows the results in terms of product yield, gas ratios and
632 volumetric gas composition. Figure 8 shows the gas yield in relation to the mass of biomass
633 in mmoles $g^{-1}_{biomass}$. The results show that there was negligible change in the gas yield
634 observed with the increase in catalyst preparation temperature (Table 7). The percentage
635 carbon content in the gaseous product showed negligible difference. It is evident from Table
636 7 that with the increase in catalyst calcination temperature, the catalytic activity and

637 selectivity for methane production was enhanced significantly. Also, the highest CH_4/CO_2
638 ratio was observed with the catalyst calcined at 950 °C indicating a high degree of CO_2
639 methanation and the high CH_4/CO ratio indicating complete CO methanation, inded at the
640 higher calcination temperatures, CO was not detected. The volumetric methane composition
641 in the product gas mixture reached a maximum of 82.4 vol.% at 950 °C catalyst calcination
642 temperature.

643 Figure 8 shows the gas yield results in terms of mmoles $g^{-1}_{biomass}$. The highest methane
644 yield in relation to biomass was obtained with the catalyst calcined at a temperature of 950
645 °C. The methane yield increased from 12.09 to 13.73 mmoles $g^{-1}_{biomass}$ with the increase in
646 calcination temperature from 650 to 950 °C. Consequently, the CO and CO_2 yields were
647 reduced due to methanation of the carbon oxides from 8.9 to 0.0 mmoles $g^{-1}_{biomass}$ for CO and
648 4.05 to 2.93 mmoles $g^{-1}_{biomass}$ for CO_2. Similar results have been reported by Zhang et al., [52]
649 for CO_2 methanation over a nickel-alumina catalyst. They calcined the alumina support at
650 600, 800 and 1000 °C before impregnation with nickel metal. They concluded that the
651 calcination temperature plays an important role in the catalytic activity. They reported the
652 highest catalytic activity for the alumina support calcined at 1000 °C. Gao et al., [53]
653 investigated the effect of catalyst calcination temperature on CO methanation in the
654 calcination temperature range of 600 °C to 1200 °C in relation to nickel-alumina catalysts.
655 They reported that the highest catalytic activity was shown by the catalyst calcined at a
656 temperature of 1200 °C. They suggested that the lower activity of the catalyst calcined at 600
657 °C was due to the presence of metal which was oxidized easily compared to that of catalyst
658 calcined at 1200 °C because of its lower stability towards oxidation. According to Bukhari et
659 al., [54] strong interaction between metal and support increases catalytic activity and results
660 in higher conversion of CO_2 to CH_4.

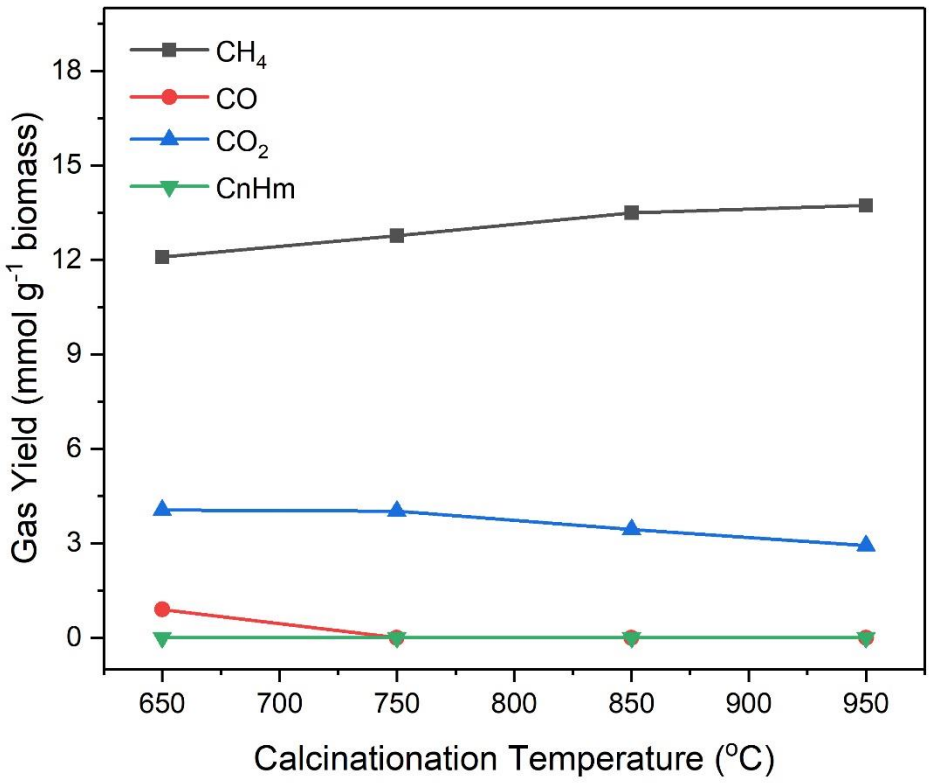

Figure 8 Influence of catalyst calcination temperature on gas yield (Pyrolysis temperature 800 °C, Catalytic steam reforming temperature 800 °C, Steam WHSV5 mL h^{-1} $g^{-1}_{catalyst}$, Catalytic hydrogenation temperature 350 °C, and Hydrogen space velocity 2400 mL $h^{-1}_{catalyst}$).

3.3.3. Influence of catalyst nickel loading for catalytic hydrogenation

The influence of the amount of nickel metal loaded onto the alumina support material was investigated to determine the influence on methane production from biomass using the three stage (i) pyrolysis (ii) catalytic steam reforming (iii) catalytic hydrogenation reactor system. The nickel loadings of 5, 10 and 15 wt.% on alumina were prepared and calcined at the catalyst calcination temperature of 950 °C and then investigated using the catalytic hydrogenation reactor. The prepared catalysts were characterized using SEM-EDXS mapping to investigate the morphology and the distribution of metal on the support and XRD analysis

675 was performed to investigate the crystallinity and metal size. The results of SEM-EDXS
676 mapping are shown in Figure 9, which suggests that the nickel metal particles were more
677 uniformly distributed in the 5 wt.% and 10 wt.% Ni/Al_2O_3 catalysts. While there is evidence
678 that sintering and non-uniform distribution could be observed with the 15 wt. % Ni/Al_2O_3.

679 The crystal structure and metal particle size were investigated using XRD analysis as
680 shown in Figure 10. For all the catalysts investigated, diffraction peaks at 2-theta 39.2°,
681 31.6°, 45.5°, 60.34, and 66.42° represents the alumina phase diffraction peaks while the
682 diffraction peaks at 2-theta 37.4°, 44.3°,51.68°, and 76.24° represents the metallic nickel
683 peaks. Figure 10 shows that with the increase in the percentage nickel loading the peak
684 intensity becomes more intense showing a more crystalline structure. In addition, the
685 crystallite size of metal was calculated using Scherrer equation and showed that the average
686 particle size for the 5 wt.%, 10 wt.% and 15 wt.% nickel loadings were 7.0, 10.2 and 12.3
687 nm. Therefore the increase in metal loading from 5 to 15 wt.% produced an increased nickel
688 crystallite size and resulted in a less uniform distribution of metal particles on the support.

689 The Ni/Al_2O_3 catalysts with different nickel metal loadings were used in the 3rd stage
690 catalytic hydrogenation reactor to investigate the influence on methane yield. The catalytic
691 hydrogenation reactor temperature was fixed at 350 °C with hydrogen space velocity of 2400
692 mL h^{-1} $g^{-1}_{catalyst}$. Table 8 shows the results in relation to nickel metal loading in terms of gas
693 yield, gas ratios and volumetric gas composition. Also, the gas yield in relation to the mass of
694 biomass in mmoles $g^{-1}_{biomass}$ is reported in Figure 11.

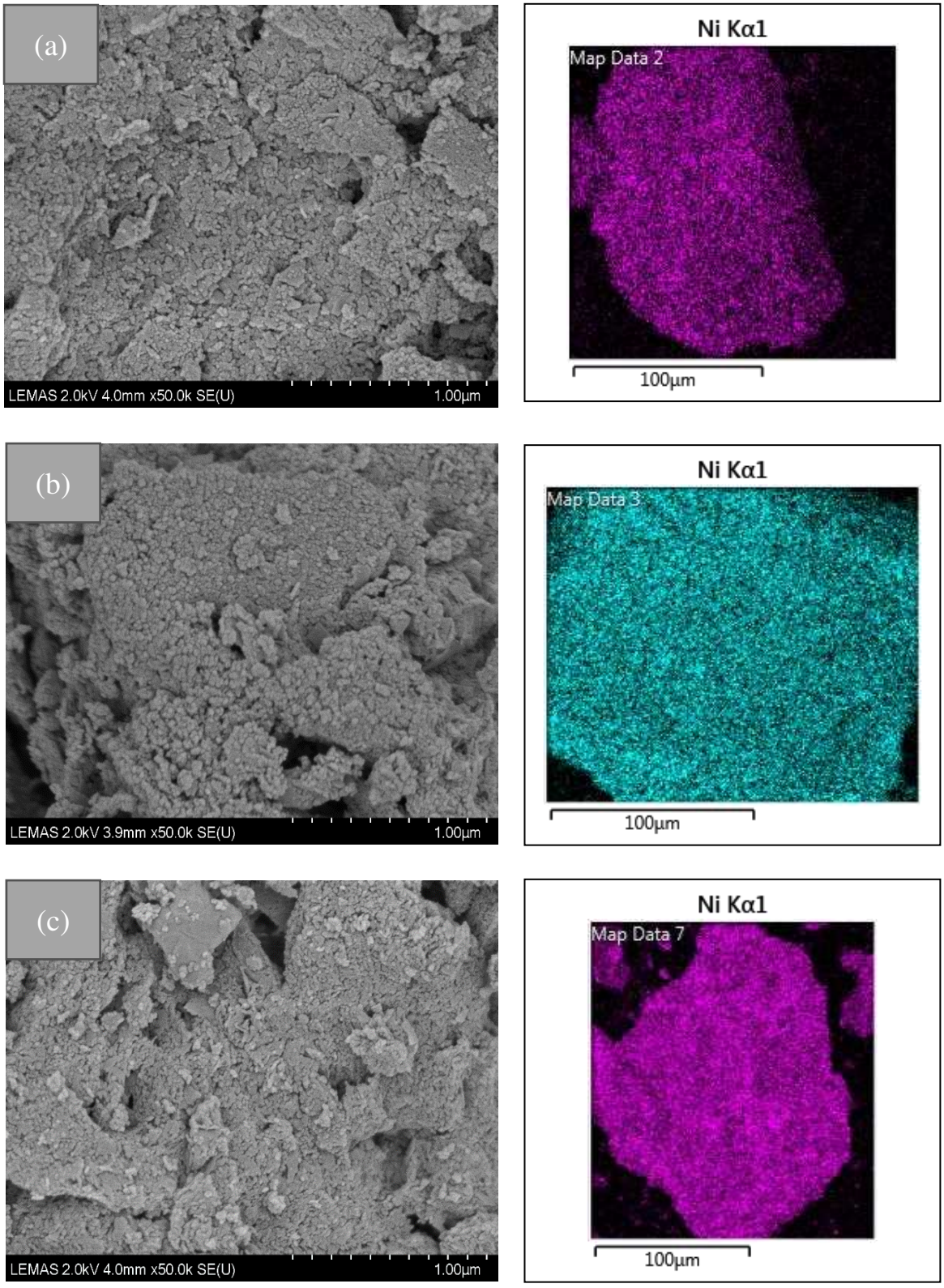

695

696 **Figure 9** SEM-EDXS analysis of various nickel loadings on alumina support a) 5 wt.

697 % Ni/Al_2O_3 b) 10 wt. % Ni/Al_2O_3 c) 15 wt. % Ni/Al_2O_3.

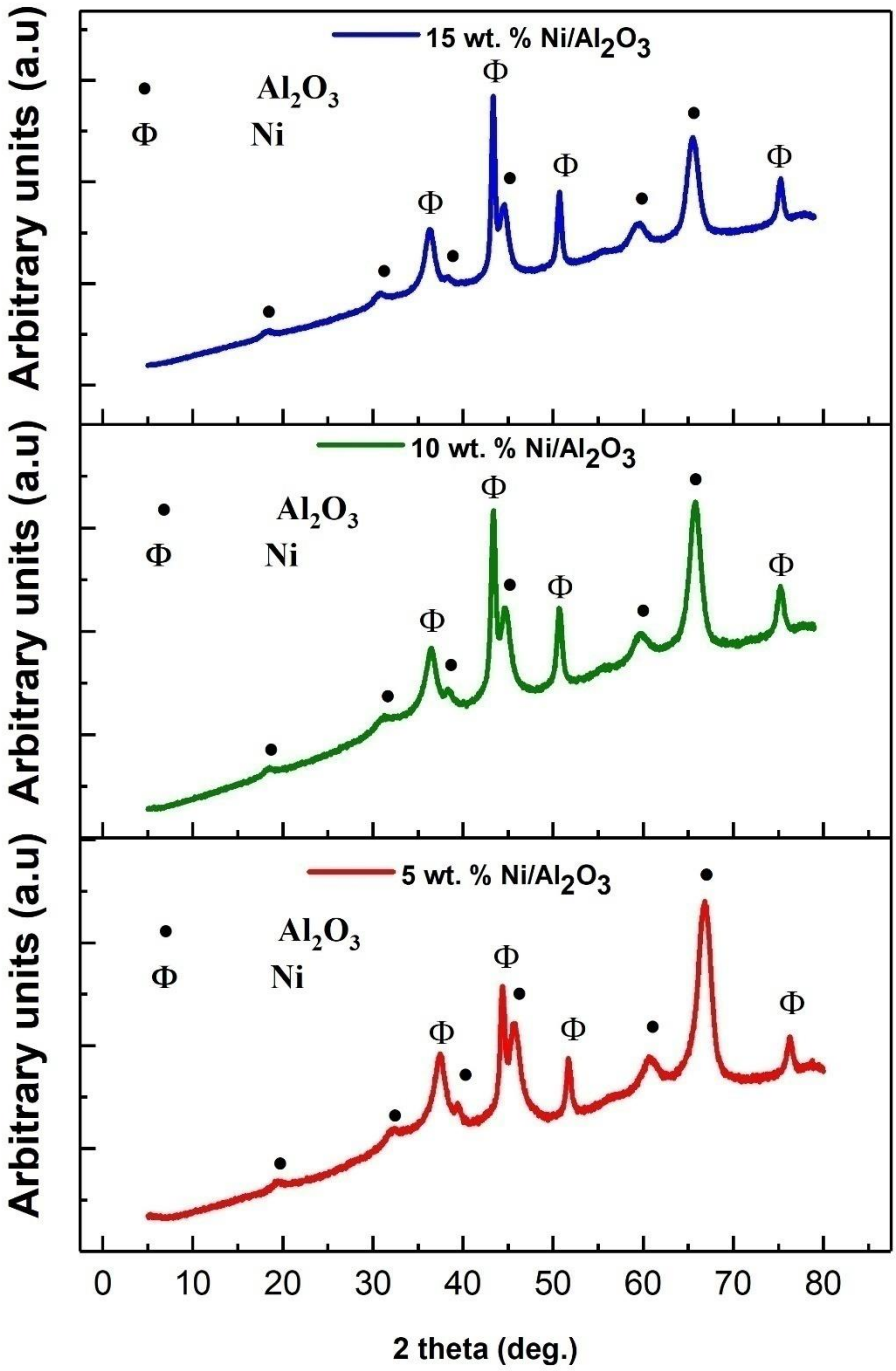

698

699 **Figure 10** XRD analysis of various nickel loadings on alumina support.

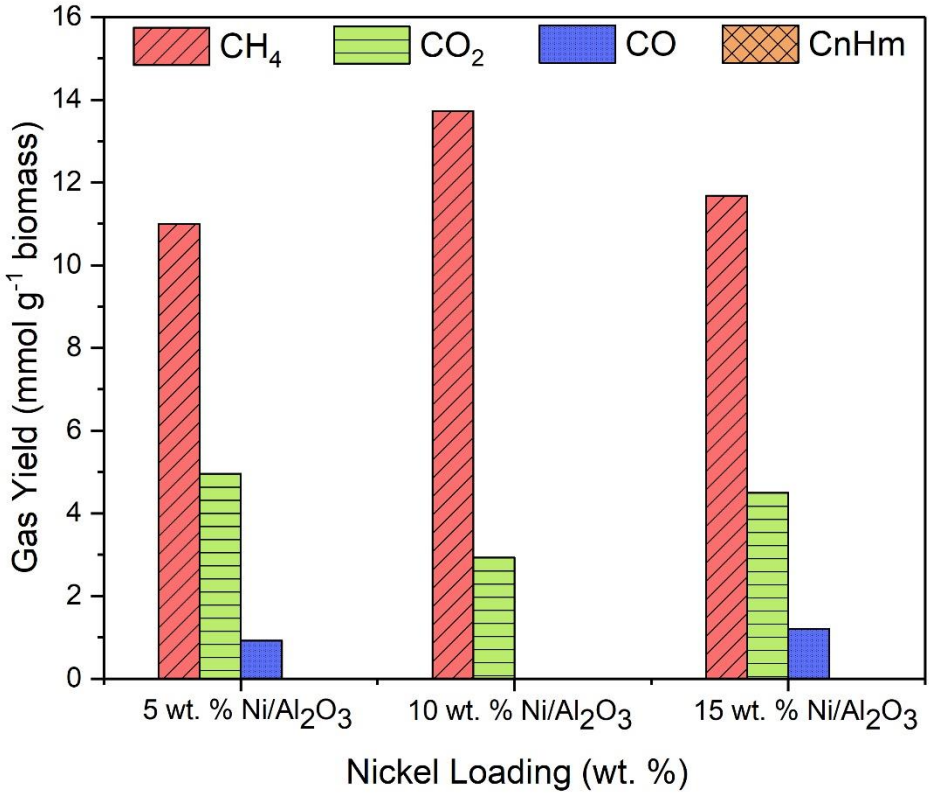

700

701 **Figure 11** Influence of metal loadings on gas yield (Pyrolysis temperature 800 °C, Catalytic
702 steam reforming temperature 800 °C, Steam WHSV5mL h^{-1} $g^{-1}_{catalyst}$, Catalytic hydrogenation
703 temperature 350 °C, and Hydrogen space velocity 2400 mL h^{-1} $g^{-1}_{catalyst}$).

704 The results in Table 8 in relation to CH_4/CO_2 ratio CH_4/CO ratio suggest that the
705 optimum nickel loading was 10 wt.% of nickel, also, it can be seen that the highest produced
706 water, suggesting the highest the promotion of the methanation reaction. Table 8 shows there
707 was insignificant difference observed in percentage carbon content of the gaseous products. It
708 can be seen that with the increase in metal loading from 5 to 10 wt.% the volumetric methane
709 concentration in the product gaseous mixture was the highest at 82.47 vol.% for the catalyst
710 with 10 wt.% nickel.

711 Figure 11 shows that with increasing the nickel loading from 5 to 10 wt.% methane
712 yield increased from 10.99 to 13.73 mmoles $g^{-1}_{biomass}$ with the reduction in CO and CO_2 yield
713 from 0.925 to 0.0mmoles $g^{-1}_{biomass}$ and 4.95 to 2.93 mmoles $g^{-1}_{biomass}$ respectively. But, at 15

wt.% of nickel loading on the alumina support the methane yield was reduced to 11.68 mmoles $g^{-1}_{biomass}$ and CO and CO_2 yield was increased. The results suggest the highest catalytic activity for methane production was with the 10 wt.% Ni/Al_2O_3 catalyst because of the optimum amount of nickel with uniform distribution. However, in the case of 5 wt. % nickel loading, there was not enough metal to carry out methanation of the carbon oxides. While 15 wt.% of nickel loading showed the sintering and non-uniform distribution of metal on the support which resulted in lower activity and selectivity towards the methanation reaction. Lin et al., [55] investigated the effect of the amount of nickel loading of 1, 10, 20 and 30 wt.% over Al_2O_3-ZrO_2 support material. They reported that the lowest catalytic activity in terms of CO_2 conversion was observed over the 1 wt.% Ni catalyst but, increased as the nickel loading was increased up to 20 wt.%. However, CO_2 conversion was reduced at the high nickel loading of 30 wt.%. They attributed the low catalytic activity for the 1 wt.% Ni-catalyst because of the low amount of active Ni sites for CO_2 methanation. But, at 30 wt. % a declining trend in CO_2 conversion was observed because of the agglomeration of nickel particles. Similarly, Rahmani et al., [56] investigated the effect of nickel metal loading (10, 15, 20, and 25 wt. %) on alumina support for CO_2 methanation. They concluded that an optimum metal loading is required to enhance catalytic activity. They reported that with the increase in nickel loading from 10 to 20 wt.% the catalytic activity was significantly enhanced. But, with the further increase in nickel loading to 25 wt. % the catalytic activity declined due to agglomeration of nickel metal on the alumina support.

3.3.4. Influence of support material for catalytic hydrogenation

The influence of the type of catalyst support material in relation to its influence on methane production from biomass using the three stage (i) pyrolysis (ii) catalytic steam reforming (iii)

739 catalytic hydrogenation reactor system was investigated. The support materials investigated
740 were SiO_2, MCM-41 and Al_2O_3 each having a nickel loading of 10 wt.% and calcined at a
741 calcination temperature of 950 °C. The prepared catalysts were used in the 3rd stage catalytic
742 hydrogenation reactor. The morphology of the prepared catalysts was investigated using the
743 SEM-EDXS mapping technique and reported in Figure 12. Also, XRD analysis was carried
744 out to investigate the crystallite size of the metal loaded on the support for the freshly
745 prepared catalysts. As shown in Figure 12, the nickel metal particles were more uniformly
746 distributed over the alumina support compared to the distribution over the MCM-41 and SiO_2
747 supports. Also, sintering of the nickel in the case of MCM-41 and SiO_2 was also observed as
748 shown by the crystallite particle size via XRD. The crystallinity and crystal size of the metal
749 was investigated using XRD. Figure 13 shows that for all the catalysts studied the nickel
750 peaks were observed at the diffraction angle 2-theta at 37.4°, 44.3°, 51.68° and 76.24°
751 respectively. In the case of the SiO_2 support, a silica peak was observed at 25° while MCM-
752 41 showed a silica peak at 25° and alumina peak at 60.34°. The alumina support showed five
753 diffraction peaks of alumina at 2-theta 39.2°, 31.6°, 45.5°, 60.34, and 66.42° respectively.
754 The crystallite size of nickel metal on the different supports for the freshly prepared catalysts
755 was calculated using the Scherrer equation which showed that Ni/SiO_2, Ni/MCM-41, and
756 Ni/Al_2O_3 had the particle sizes of 28.0, 13.7 and 10.2 nm respectively. The extent of the
757 distribution of the active metal on the support material depends on the interaction between
758 metal and support. Weak metal support interaction leads to the agglomeration of the metal
759 particles [57]. Oemar et al., [58] reported that weak interaction exists between Ni and SiO_2
760 supports. This weak interaction results in the formation of weakly bound NiO species which
761 generally exist in the form of larger active metal particle sizes and can easily agglomerate
762 during the reduction reaction. In most cases, a strong chemical interaction exits between Ni
763 and Al_2O_3 support and exists in the form of nickel aluminate. This results in a uniform

764 distribution of Ni particles over the alumina support [57]. However, no such chemical
765 interaction exists between Ni and SiO_2 support and an alkaline environment is required to
766 form nickel silicate [59]. Amin et al., [60] compared the metal support interaction of
767 Ni/Al_2O_3 and Ni/MCM-41 catalysts. They reported that the stronger metal support interaction
768 of the Ni/Al_2O_3 catalyst as compared to the Ni/MCM-41 catalyst was because of the presence
769 of a larger amount of nickel aluminate rather than weakly bound NiO species.

770 The influence of different catalyst support material on methane yield was carried out
771 in the three stage reactor system. The catalytic hydrogenation reactor was maintained at 350
772 °C with hydrogen space velocity at 2400 mL h^{-1} $g^{-1}_{catalyst}$. The influence of different catalyst
773 support material on gas composition, product yield and gas ratios are shown in Table 9. In
774 addition, gas yield in relation to the mass of biomass in mmoles $g^{-1}_{biomass}$ is shown in Figure
775 14.

776

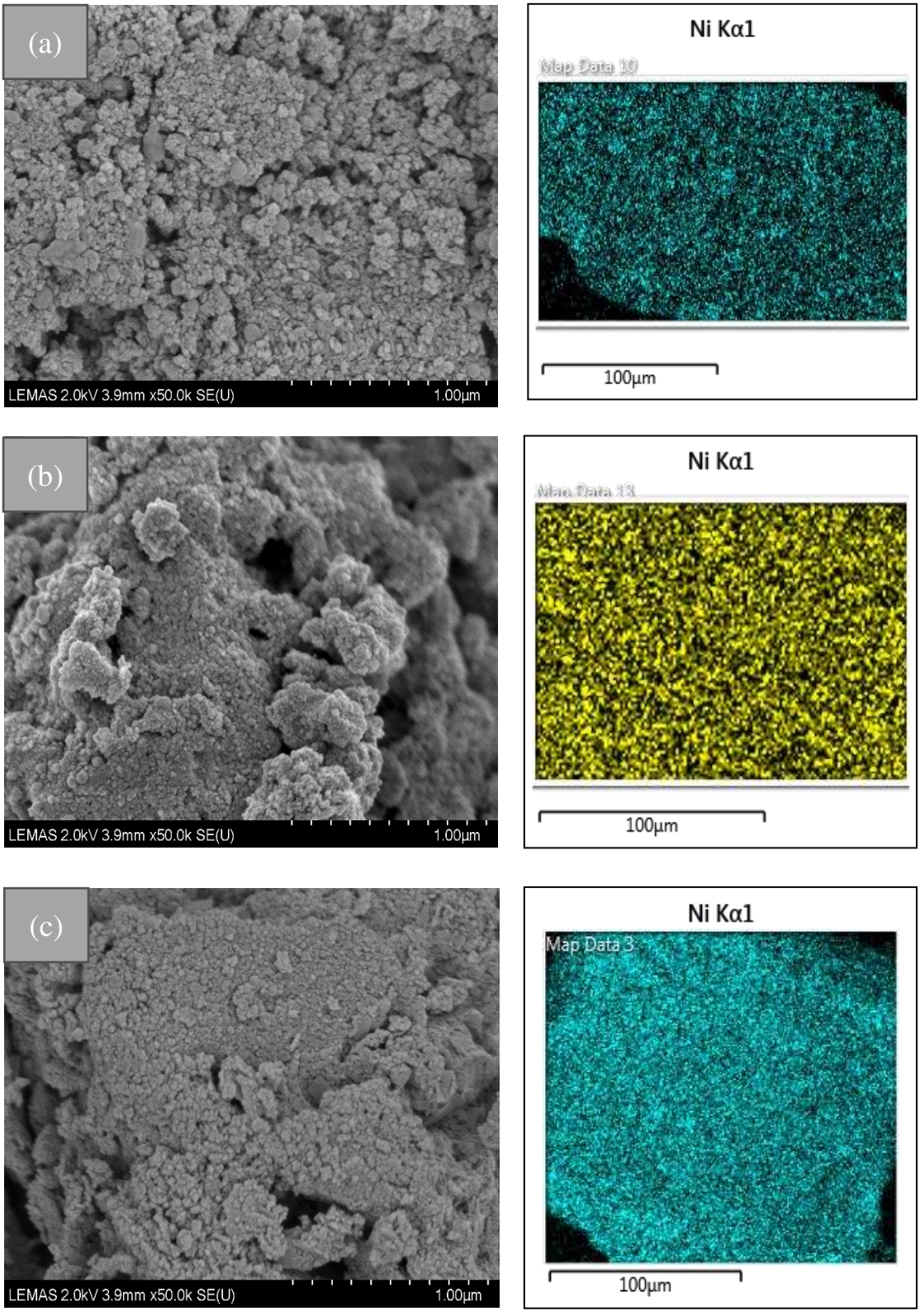

Figure 12 SEM-EDXS analysis of different catalytic supports for the freshly prepared catalysts, a) 10 wt. % Ni/SiO_2 b) 10 wt. % Ni/MCM-41 c) 10 wt. % Ni/Al_2O_3

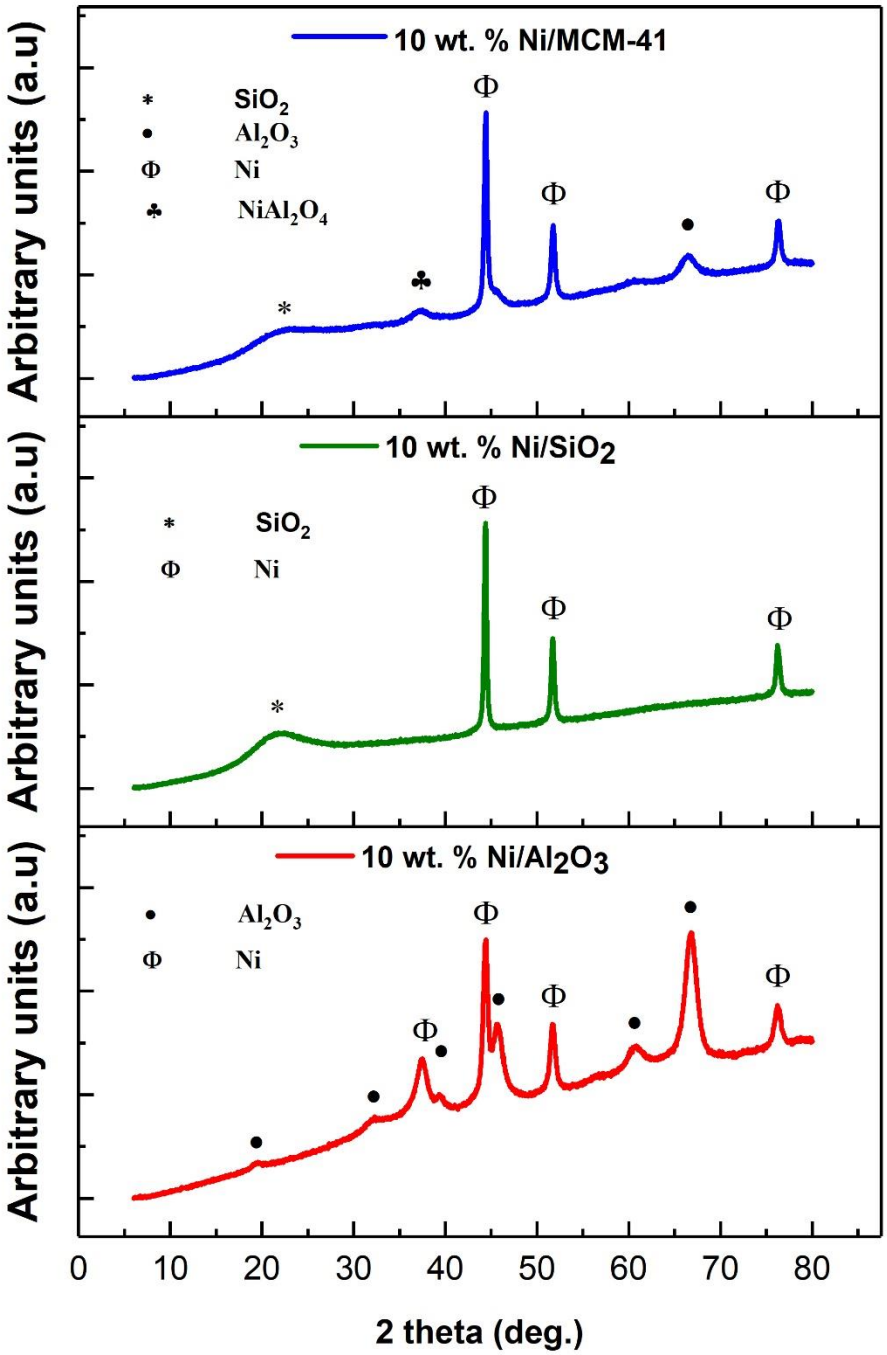

780

781 **Figure 13** XRD analysis of 10 wt. % Nickel catalyst with different supports.

782 Table 9 shows that the highest CH_4/CO and CH_4/CO_2 gas ratio was shown by the
783 alumina support. The alumina supported catalyst showed a CH_4/CO_2 ratio of 4.68 with
784 complete conversion of CO to methane. While CH_4/CO_2 and CH_4/CO ratios produced by

785 MCM-41 and SiO_2 were significantly lower suggesting the promotion of the methanation
786 reaction for the nickel-alumina catalyst compared to that of MCM-41 and SiO_2 supported
787 catalyst. Also, the highest product water as the result of methanation reaction was produced
788 with the Ni/Al_2O_3 catalyst. Which shows the promotion of methanation reaction of Ni/Al_2O_3
789 catalyst compared to that of SiO_2 and MCM-41 catalysts. There was no significant difference
790 observed in carbon content of gaseous products of different supports investigated. Table 9
791 shows that the highest volumetric methane concentration in the output gaseous mixture of
792 82.4 vol.% was obtained over Al_2O_3 supported catalyst. While MCM-41 and SiO_2 supported
793 catalyst showed much lower methane concentrations of 42.5 and 20.2 vol.% respectively. The
794 MCM-41 and SiO_2 supported catalysts also showing much higher CO and CO_2 suggesting
795 lower carbon oxide methanation compared to the alumina supported catalyst

796 The influence of the different supported catalysts, Ni/SiO_2, Ni/MCM-41, and
797 Ni/Al_2O_3 on gas yield is shown in Figure 14. The highest methane yield of 13.73 mmoles $g^{-1}_{biomass}$
798 was obtained with the alumina supported nickel catalyst followed by MCM-41 at
799 7.821 mmoles $g^{-1}_{biomass}$ and SiO_2 at 3.764 mmoles $g^{-1}_{biomass}$. The SiO_2 and MCM-41 supports
800 showed significantly higher CO_2 and CO yields compared to the low CO_2 and CO
801 yieldsproduced for the alumina support due to the more enhanced carbon oxides
802 hydrogenation. The CO_2 and CO conversion to methane via the methanation reaction for the
803 nickel catalysts with different supports was in the order Al_2O_3> MCM-41> SiO_2. There are
804 reports that the presence of water markedly reduces the catalytic activity of MCM-41because
805 of enhanced sintering of the catalyst metal [61-63]. The lower conversion of CO_2 and CO
806 may be attributed to the larger crystallite particle size and non-uniform distribution of Ni
807 metal over SiO_2 and particularly the MCM-41 support compared to that of the alumina
808 support which was evident from SEM-EDXS and XRD results. The used catalysts after
809 reaction were characterised using XRD analysis and SEM-EDXS.to determine any evidence of

sintering. The calculated particle size of the used 10 wt. % Ni/Al_2O_3, 10 wt. % Ni/SiO_2 and 10 wt. % Ni/MCM-41 catalysts were 11.1 nm, 26.7 nm and 12.8 nm which compared with the particle size of the fressh catalysts as 10.2 nm, 28.0, and 13.7 nm respectively. That is, no significant change in the metal particle size was observed for all the catalyst studied. In addition, no notable change in surface morphology was observed on reviewing the SEM-EDXS results attained for all catalyst supports. This suggests that the catalysts were resistant to sintering during the catalytic hydrogenation because of the high preparation calcination temperature which enhanced the catalyst stability

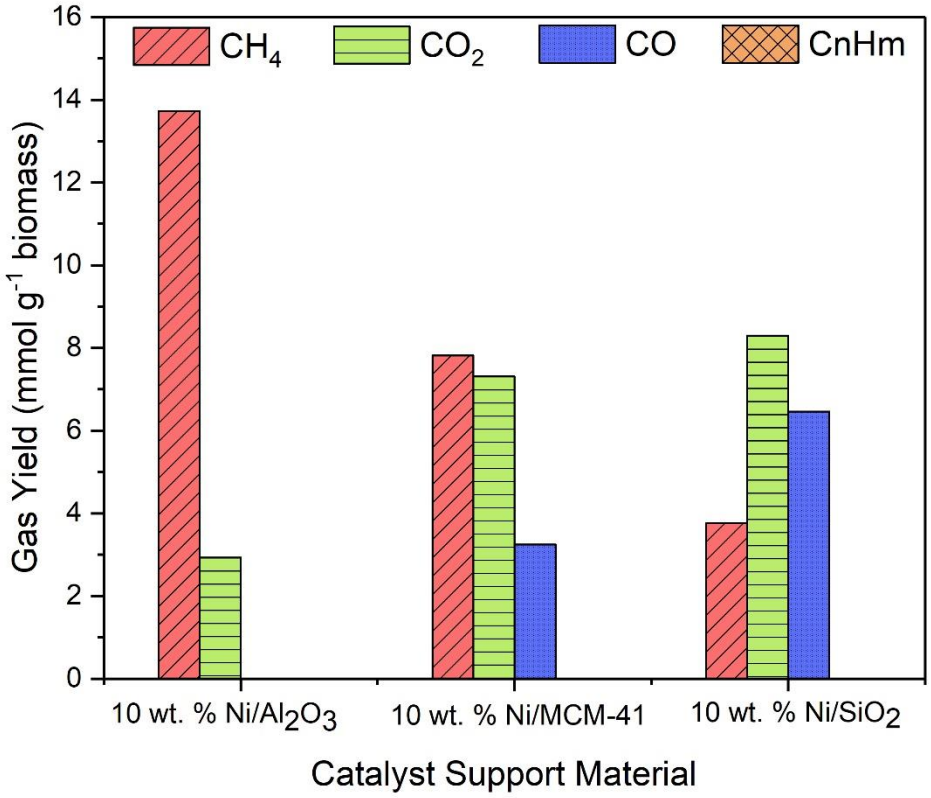

Figure 14 Influence of different catalyst supports on gas yield (Pyrolysis temperature 800 °C, Catalytic steam reforming temperature 800 °C, Steam WHSV5 mL h^{-1} $g^{-1}_{catalyst}$, Catalytic hydrogenation temperature 350 °C, and Hydrogen space velocity 2400 mL h^{-1} g^{-1} catalyst).

3.4. Comparison of the two-stage and three stage processes

Our previous work [19] focussed on methane production from biomass using a two-stage (i) pyrolysis (ii) catalytic hydrogenation reactor system. This current work has investigated methane production from biomass using a three stage (i) pyrolysis (ii) catalytic steam reforming (iii) catalytic hydrogenation reactor system. In the three stage process, the optimum stage two (ii) catalytic steam reforming temperature was 800 °C steam WHSV of 5 mL h^{-1} $g^{-1}_{catalyst}$ and optimum stage three (iii) catalytic hydrogenation temperature was 350 °C with hydrogen space velocity of 2400 mL h^{-1} $g^{-1}_{catalyst}$. While for the two-stage process the optimum stage two (ii) catalytic hydrogenation temperature was 500 °C with hydrogen space velocity of 3600 mL h^{-1} $g^{-1}_{catalyst}$.

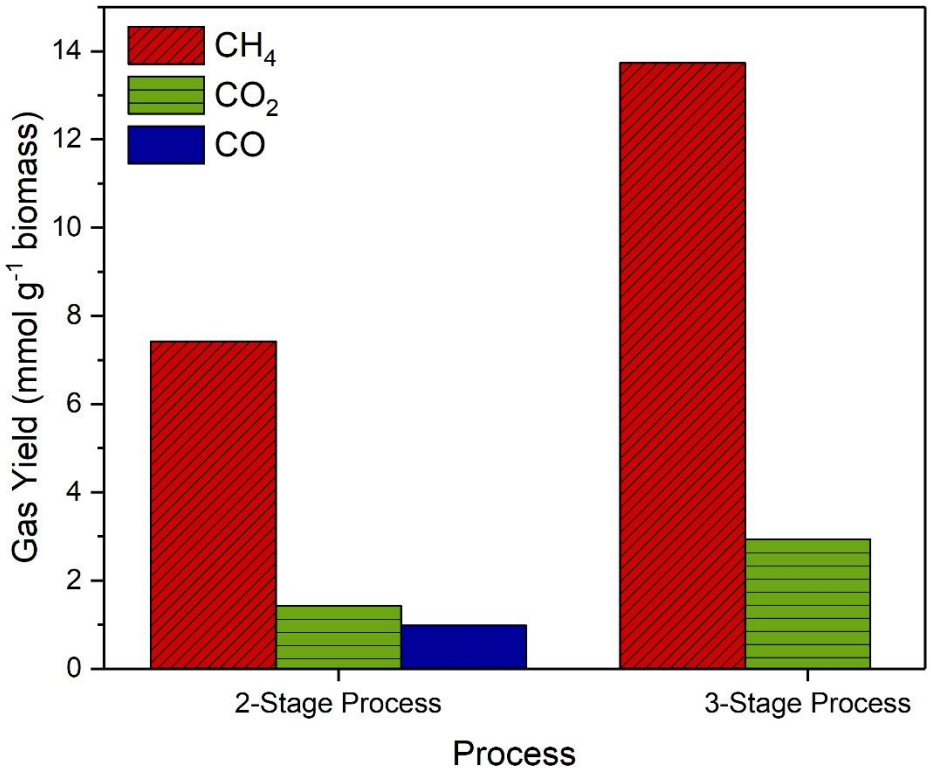

Figure 15 Comparison of the gas yields obtained from the two-stage and three-stage processes at the optimized conditions.

As shown in Figure 15, after optimizing operating parameters the stage three process resulted in a 1.8 fold higher methane yield compared to that of the two stage process because of the formation and conversion of more CO and CO_2 during the reforming and methanation processes. The methane yield obtained from the two-stage pyrolysis-catalytic hydrogenation reactor system was 7.41 mmoles $g^{-1}_{biomass,}$ ~11.88 g CH_4 100 $g^{-1}_{biomass}$ while the methane yield obtained using the three stage pyrolysis-catalytic steam reforming-catalytic hydrogenation system was 13.73 mmoles $g^{-1}_{biomass}$, representing 22.02 g CH_4 100 $g^{-1}_{biomass}$. A 100 % conversion of CO was achieved in the three-stage process while for the two-stage process, CO was obtained in the ouput gaseous mixture. This was because the catalytic hydrogenation was carried out at higher temperature which favours the reverse water gas shift reaction. Upon optimization of hydrogen space velocity, the three-stage process resulted in the highest methane yield of 12.77 mmoles $g^{-1}_{biomass}$, (20.48 g CH_4 100 $g^{-1}_{biomass}$) at 2400 mL h^{-1} $g^{-1}_{catalyst}$, while the two-stage process yielded a highest methane yield of 5.08 mmoles $g^{-1}_{biomass}$ (8.14 g CH_4 100 $g^{-1}_{biomass}$) at 3600 mL h^{-1} $g^{-1}_{catalyst}$. This shows higher input hydrogen space velocity is required to enhance the methanation reaction in the two-stage process compared to that of the three-stage process. This was because the three-stage process produced hydrogen during the catalytic steam reforming process to undertake COx methanation. Therefore it can be concluded that the three-stage process is an efficient process for methane production.

4.0 CONCLUSIONS

In this work, a detailed study of operating parameters and catalyst characteristics has been carried out to maximise methane yield from biomass using a three stage (i) pyrolysis (ii) catalytic steam reforming (iii) catalytic hydrogenation reactor system. The main conclusions of this study are the following;

A suitable high catalytic steam reforming temperature is required to convert all the higher hydrocarbons into low molecular weight gaseous product i.e. CO, CO_2 and H_2. The conversion of higher molecular weight pyrolysis hydrocarbons into low molecular weight species was obtained at higher catalyst temperatures (800-900 °C). At lower reforming temperatures, formation of liquid bio-oil and high molecular weight hydrocarbons occurred. An optimum steam WHSV for product pyrolysis gas reforming is also required to enhance the conversion of higher molecular weight hydrocarbons.

An optimum catalytic hydrogenation reactor temperature is required to convert the COx into methane. Higher temperatures resulted in the suppression of methanation reactions because of the promotion of the reverse water gas shift reaction (RWGS). An optimum hydrogen space velocity is also required to convert COx into methane. Higher hydrogen space velocity resulted in insufficient contact time between the reactant gases and the catalyst and resulted in lower conversion of COx. Among different metal catalysts loaded on the alumina support material, Ni metal showed the highest catalytic activity in terms of COx conversion. The catalytic activity of various metal catalysts decreased in the following order Ni > Co > Fe > Mo. Increase in catalyst calcination temperature for the preparation of 10 wt. % Ni/Al_2O_3 resulted in an increase in COx conversion because of the increase in metal support interaction. A suitable amount of metal loading is required to enhance catalytic activity. Low metal loading decreases the COx conversion because of the absence of a sufficient amount of active metal to carry out methanation. Higher metal loading resulted in the agglomeration of metal particles which decreased catalytic activity. Among the different support materials investigated Al_2O_3 support showed the highest catalytic activity because of the uniform distribution of metal particles and resistance to sintering. While SiO_2 and MCM-41 showed a non-uniform distribution of metal particles and less resistance to sintering. The

887 catalytic activity of the different supports investigated was in the following order Al_2O_3>
888 MCM-41 > SiO_2.

889 **REFERENCES**

890 1. ADEKOYA, D., M. TAHIR and N.A.S. AMIN. Recent trends in photocatalytic materials for
891 reduction of carbon dioxide to methanol. *Renewable and Sustainable Energy Reviews*, 2019,
892 **116**, p.109389.

893 2. NIU, M., Y. HUANG, B. JIN, S. LIANG, Q. DONG, H. GU and R. SUN. A novel two-stage
894 enriched air biomass gasification for producing low-tar high heating value fuel gas: Pilot
895 verification and performance analysis. *Energy*, 2019, **173**, pp.511-522.

896 3. SAFARIAN, S., R. UNNÞÓRSSON and C. RICHTER. A review of biomass gasification
897 modelling. *Renewable and Sustainable Energy Reviews*, 2019, **110**, pp.378-391.

898 4. JAHIRUL, M.I., M.G. RASUL, A.A. CHOWDHURY and N.J.E. ASHWATH. Biofuels
899 production through biomass pyrolysis—a technological review. 2012, **5**(12), pp.4952-5001.

900 5. HERVY, M., R. OLCESE, M.M. BETTAHAR, M. MALLET, A. RENARD, L.
901 MALDONADO, D. REMY, G. MAUVIEL and A. DUFOUR. Evolution of dolomite
902 composition and reactivity during biomass gasification. *Applied Catalysis A: General*, 2019,
903 **572**, pp.97-106.

904 6. DE CASTRO, T.P., E.B. SILVEIRA, R.C. RABELO-NETO, L.E.P. BORGES and F.B.
905 NORONHA. Study of the performance of Pt/Al_2O_3 and $Pt/CeO_2/Al_2O_3$ catalysts for steam
906 reforming of toluene, methane and mixtures. *Catalysis Today*, 2018, **299**, pp.251-262.

907 7. YAMAGUCHI, A., N. HIYOSHI, O. SATO, K.K. BANDO, M. OSADA and M. SHIRAI.
908 Hydrogen production from woody biomass over supported metal catalysts in supercritical
909 water. *Catalysis Today*, 2009, **146**(1), pp.192-195.

910 8. LAPRUNE, D., D. FARRUSSENG, Y. SCHUURMAN, F.C. MEUNIER, J.A.Z. PIETERSE,
911 A.M. STEELE and S. THORPE. Effects of H2S and phenanthrene on the activity of Ni and
912 Rh-based catalysts for the reforming of a simulated biomass-derived producer gas. *Applied*
913 *Catalysis B: Environmental*, 2018, **221**, pp.206-214.

914 9. CHEN, G., J. LI, C. LIU, B. YAN, Z. CHENG, W. MA, J. YAO and H. ZHANG. Low-
915 Temperature Catalytic Cracking of Biomass Gasification Tar Over Ni/HZSM-5. *Waste and*
916 *Biomass Valorization*, 2019, **10**(4), pp.1013-1020.

917 10. SANTAMARIA, L., A. ARREGI, G. LOPEZ, M. ARTETXE, M. AMUTIO, J. BILBAO and
918 M. OLAZAR. Effect of La_2O_3 promotion on a Ni/Al_2O_3 catalyst for H_2 production in the in-
919 line biomass pyrolysis-reforming. *Fuel*, 2020, **262**, p.116593.

920 11. SHANMUGANANDAM, K. and M.V. RAMANAN. Ni-Ce/SiO2 nanocomposite:
921 Characterization and catalytic activity in the cracking of tar in biomass gasifiers. *Energy*
922 *Sources, Part A: Recovery, Utilization, and Environmental Effects*, 2016, **38**(16), pp.2418-
923 2425.

924 12. NEJAT, T., P. JALALINEZHAD, F. HORMOZI and Z. BAHRAMI. Hydrogen production
925 from steam reforming of ethanol over Ni-Co bimetallic catalysts and MCM-41 as support.
926 *Journal of the Taiwan Institute of Chemical Engineers*, 2019, **97**, pp.216-226.

927 13. GRAMS, J., R. RYCZKOWSKI, K. CHAŁUPKA, I. SOBCZAK, I. RZEŹNICKA and
928 K.J.M. PRZYBYSZ. Impact of Support (MCF, ZrO2, ZSM-5) on the Efficiency of Ni
929 Catalyst in High-Temperature Conversion of Lignocellulosic Biomass to Hydrogen-Rich Gas.
930 Materials, 2019, **12**(22), p.3792.

14. WU, C., P.T. WILLIAMS. Nickel-based catalysts for tar reduction in biomass gasification. *Biofuels*, 2011, **2**(4), pp.451-464.

15. CHANG, F.W., M.S. KUO, M.T. TSAY, M.C HSIEH, E. . Effect of calcination temperature on catalyst reducibility and hydrogenation reactivity in rice husk ash–alumina supported nickel systems. Journal of Chemical Technology and Biotechnology, 2004, **79**(7), pp.691-699.

16. BACARIZA, M.C., I. GRAÇA, S.S. BEBIANO, J.M. LOPES and C. HENRIQUES. Micro- and mesoporous supports for CO2 methanation catalysts: A comparison between SBA-15, MCM-41 and USY zeolite. *Chemical Engineering Science*, 2018, **175**, pp.72-83.

17. GARBARINO, G., C. WANG, T. CAVATTONI, E. FINOCCHIO, P. RIANI, M. FLYTZANI-STEPHANOPOULOS and G. BUSCA. A study of Ni/La-Al2O3 catalysts: A competitive system for CO2 methanation. *Applied Catalysis B: Environmental*, 2019, **248**, pp.286-297.

18. PANAGIOTOPOULOU, P. Hydrogenation of CO2 over supported noble metal catalysts. Applied Catalysis A: General 2017, **542**, pp.63-70.

19. JAFFAR, M.M., M.A. NAHIL and P.T. WILLIAMS. Methane Production from the Pyrolysis–Catalytic Hydrogenation of Waste Biomass: Influence of Process Conditions and Catalyst Type. *Energy & Fuels*, 2019, **33**(8), pp.7443-7457.

20. YOON, H.C., T. COOPER and A. STEINFELD. Non-catalytic autothermal gasification of woody biomass. *International Journal of Hydrogen Energy*, 2011, **36**(13), pp.7852-7860.

21. CHUANG, K.-H., B.-N. CHEN and M.-Y. WEY. Enrichment of Hydrogen Production from Biomass-Gasification-Derived Syngas over Spinel-Type Aluminate-Supported Nickel Catalysts. 2018, **6**(2), pp.318-325.

22. HU, M., L. GAO, Z. CHEN, C. MA, Y. ZHOU, J. CHEN, S. MA, M. LAGHARI, B. XIAO, B. ZHANG and D. GUO. Syngas production by catalytic in-situ steam co-gasification of wet sewage sludge and pine sawdust. *Energy Conversion and Management*, 2016, **111**, pp.409-416.

23. LUO, S., B. XIAO, X. GUO, Z. HU, S. LIU and M. HE. Hydrogen-rich gas from catalytic steam gasification of biomass in a fixed bed reactor: Influence of particle size on gasification performance. *International Journal of Hydrogen Energy*, 2009, **34**(3), pp.1260-1264.

24. GAO, N., A. LI and C. QUAN. A novel reforming method for hydrogen production from biomass steam gasification. *Bioresource Technology*, 2009, **100**(18), pp.4271-4277.

25. WAHEED, Q.M.K. and P.T. WILLIAMS. Hydrogen Production from High Temperature Pyrolysis/Steam Reforming of Waste Biomass: Rice Husk, Sugar Cane Bagasse, and Wheat Straw. *Energy & Fuels*, 2013, **27**(11), pp.6695-6704.

26. AKUBO, K., M.A. NAHIL and P.T. WILLIAMS. Pyrolysis-catalytic steam reforming of agricultural biomass wastes and biomass components for production of hydrogen/syngas. *Journal of the Energy Institute*, 2019, **92**(6), pp.1987-1996.

27. FRANCO, C., F. PINTO, I. GULYURTLU, and I. CABRITA.The study of reactions influencing the biomass steam gasification process☆. Fuel, 2003. **82**(7): p. 835-842.

28. QUAN, C., S. XU, and C. ZHOU.Steam reforming of bio-oil from coconut shell pyrolysis over Fe/olivine catalyst. Energy Conversion and Management, 2017. **141**: p. 40-47.

29. LI, J., Y. YIN, X. ZHANG, J. LIU and R. YAN. Hydrogen-rich gas production by steam gasification of palm oil wastes over supported tri-metallic catalyst. *International Journal of Hydrogen Energy*, 2009, **34**(22), pp.9108-9115.

30. Jaffar, M.M., M.A. Nahil, and P.T. Williams, Parametric Study of CO2 Methanation for Synthetic Natural Gas Production. Energy Technology, 2019. **7**(11): p. 1900795.

31. LU, H., X. YANG, G. GAO, J. WANG, C. HAN, X. LIANG, C. LI, Y. LI, W. ZHANG, X. CHEN. Metal (Fe, Co, Ce or La) doped nickel catalyst supported on ZrO2 modified mesoporous clays for CO and CO2 methanation. *Fuel*, 2016, **183**, pp.335-344.

32. RAHMANI, S., M. REZAEI and F. MESHKANI. Preparation of promoted nickel catalysts supported on mesoporous nanocrystalline gamma alumina for carbon dioxide methanation reaction. *Journal of Industrial and Engineering Chemistry*, 2014, **20**(6), pp.4176-4182.

33. ZHANG, Z., Y. TIAN, L. ZHANG, S. HU, J. XIANG, Y. WANG, L. XU, Q. LIU, S. ZHANG and X. HU. Impacts of nickel loading on properties, catalytic behaviors of Ni/γ–Al2O3 catalysts and the reaction intermediates formed in methanation of CO2. *International Journal of Hydrogen Energy*, 2019, **44**(18), pp.9291-9306.

34. LI, Y., Q. ZHANG, R. CHAI, G. ZHAO, F. CAO, Y. LIU and Y. LU. Metal-foam-structured Ni–Al2O3 catalysts: Wet chemical etching preparation and syngas methanation performance. *Applied Catalysis A: General*, 2016, **510**, pp.216-226.

35. PASTOR-PÉREZ, L., E.L. SACHÉ, C. JONES, S. GU, H. ARELLANO-GARCIA , T.R. REINA. Synthetic natural gas production from CO2 over Ni-x/CeO2-ZrO2 (x = Fe, Co) catalysts: Influence of promoters and space velocity. *Catalysis Today*, 2018, **317**, pp.108-113.

36. KANG, W.R. and K.B. LEE. Effect of operating parameters on methanation reaction for the production of synthetic natural gas. *Korean Journal of Chemical Engineering*, 2013, **30**(7), pp.1386-1394.

37. HUSSAIN, I., A.A. JALIL, C.R. MAMAT, T.J. SIANG, A.F.A. RAHMAN, M.S. AZAMI, R.H. ADNAN. New insights on the effect of the H2/CO ratio for enhancement of CO methanation over metal-free fibrous silica ZSM-5: Thermodynamic and mechanistic studies. *Energy Conversion and Management*, 2019, **199**, p.112056.

38. GAO, J., Y. WANG, Y. PING, D. HU, G. XU, F. GU and F.J.R.A. SU. A thermodynamic analysis of methanation reactions of carbon oxides for the production of synthetic natural gas. 2012, **2**(6), pp.2358-2368.

39. FISCHER, F., H. TROPSCH, and P. DILTHEY.Reduction of carbon monoxide to methane in the presence of various metals. Brennstoff-chemie, 1925. **6**: p. 265-271.

40. SAITO, M. and R.B. ANDERSON.The activity of several molybdenum compounds for the methanation of CO. Journal of Catalysis, 1980. **63**(2): p. 438-446.

41. REN, J., QIN, X., J. -Z. YANG, Z. -F. QIN, H. -L. GUO, J. -Y. LIN, andZ. LI. Methanation of carbon dioxide over Ni–M/ZrO2 (M=Fe, Co, Cu) catalysts: Effect of addition of a second metal. Fuel Processing Technology, 2015. **137**: p. 204-211.

42. KONISHCHEVA, M.V., D.I. POTEMKIN, P.V. SNYTNIKOV, M.M. ZYRYANOVA, V.P. PAKHARUKOVA, P.A. SIMONOV and V.A. SOBYANIN. Selective CO methanation in

H2-rich stream over Ni–, Co– and Fe/CeO2: Effect of metal and precursor nature. *International Journal of Hydrogen Energy*, 2015, **40**(40), pp.14058-14063.

43. TAKENAKA, S., T. SHIMIZU and K. OTSUKA. Complete removal of carbon monoxide in hydrogen-rich gas stream through methanation over supported metal catalysts. *International Journal of Hydrogen Energy*, 2004, **29**(10), pp.1065-1073.

44. HUO, X., Z. WANG, J. HUANG, R. ZHANG and Y. FANG. Bulk Mo and Co–Mo carbides as catalysts for methanation. *Catalysis Communications*, 2016, **79**, pp.39-44.

45. AZIZ, M., A. JALIL, S. TRIWAHYONO and S.J.A.C.A.G. SIDIK. Methanation of carbon dioxide on metal-promoted mesostructured silica nanoparticles. 2014, **486**, pp.115-122.

46. ALRAFEI, B., I. POLAERT, A. LEDOUX and F. AZZOLINA-JURY. Remarkably stable and efficient Ni and Ni-Co catalysts for CO2 methanation. *Catalysis Today*, 2019.

47. PANDEY, D., K. RAY, R. BHARDWAJ, S. BOJJA, K.V.R. CHARY and G. DEO. Promotion of unsupported nickel catalyst using iron for CO2 methanation. *International Journal of Hydrogen Energy*, 2018, **43**(10), pp.4987-5000.

48. LIU, Q., B. BIAN, J. FAN and J. YANG. Cobalt doped Ni based ordered mesoporous catalysts for CO2 methanation with enhanced catalytic performance. *International Journal of Hydrogen Energy*, 2018, **43**(10), pp.4893-4901.

49. YAO, L., Y. WANG, M.E. GALVEZ, C. HU and P.J.M.R.I.C. DA COSTA. γ-Alumina-Supported Ni-Mo Carbides as Promising Catalysts for CO2 Methanation. 2017, **6**(4), pp.135-145.

50. WEI, W. and G. JINLONG. Methanation of carbon dioxide: an overview. Frontiers of Chemical Science and Engineering, 2011, **5**(1), pp.2-10.

51. ALJISHI, A., G. VEILLEUX, J.A.H. LALINDE and J. KOPYSCINSKI. The effect of synthesis parameters on ordered mesoporous nickel alumina catalyst for CO2 methanation. *Applied Catalysis A: General*, 2018, **549**, pp.263-272.

52. ZHANG, Z., T. WEI, G. CHEN, C. LI, D. DONG, W. WU, Q. LIU and X. HU. Understanding correlation of the interaction between nickel and alumina with the catalytic behaviors in steam reforming and methanation. *Fuel*, 2019, **250**, pp.176-193.

53. GAO, J., C. JIA, J. LI, M. ZHANG, F. GU, G. XU, Z. ZHONG and F. SU. Ni/Al2O3 catalysts for CO methanation: Effect of Al2O3 supports calcined at different temperatures. *Journal of Energy Chemistry*, 2013, **22**(6), pp.919-927.

54. BUKHARI, S.N., C.C. CHONG, H.D. SETIABUDI, N. AINIRAZALI, M.A.A. AZIZ, A.A. JALIL and S.Y. CHIN. Optimal Ni loading towards efficient CH4 production from H2 and CO2 over Ni supported onto fibrous SBA-15. *International Journal of Hydrogen Energy*, 2019, **44**(14), pp.7228-7240.

55. LIN, J., C. MA, Q. WANG, Y. XU, G. MA, J. WANG, H. WANG, C. DONG, C. ZHANG and M. DING. Enhanced low-temperature performance of CO2 methanation over mesoporous Ni/Al2O3-ZrO2 catalysts. *Applied Catalysis B: Environmental*, 2019, **243**, pp.262-272.

56. RAHMANI, S., M. REZAEI and F. MESHKANI. Preparation of highly active nickel catalysts supported on mesoporous nanocrystalline γ-Al2O3 for CO2 methanation. *Journal of Industrial and Engineering Chemistry*, 2014, **20**(4), pp.1346-1352.

57. ALAYAT, A., E. ECHEVERRIA, F. SOTOUDEHNIAKARANI, D.N. MCLLROY, andA. G. MCDONALD. Alumina Coated Silica Nanosprings (NS) Support Based Cobalt Catalysts for Liquid Hydrocarbon Fuel Production From Syngas. Materials, 2019. **12**(11): p. 1810.

58. OEMAR, U., Y. KATHIRASER, L. MO, X. HO, and S. KAWI.CO2 reforming of methane over highly active La-promoted Ni supported on SBA-15 catalysts: mechanism and kinetic modelling. Catalysis Science & Technology, 2016. **6**(4): p. 1173-1186.

59. LIU, C. J., J. YE, JIANG, andY. PAN.Progresses in the preparation of coke resistant Ni-based catalyst for steam and CO2 reforming of methane. ChemCatChem, 2011. **3**(3): p. 529-541.

60. AMIN, M.H., J. TARDIO, and S.K. BHARGAVA.A comparison study on carbon dioxide reforming of methane over Ni catalysts supported on mesoporous SBA-15, MCM-41, KIT-6 and gamma-Al2. Chemeca 2013: Challenging Tomorrow, 2013: p. 543.

61. AZIZ, M.A.A., A.A. JALIL, S. TRIWAHYONO and M.W.A. SAAD. CO2 methanation over Ni-promoted mesostructured silica nanoparticles: Influence of Ni loading and water vapor on activity and response surface methodology studies. *Chemical Engineering Journal*, 2015, **260**, pp.757-764.

62. TATSUMI, T., K.A. KOYANO, Y. TANAKA and S.J.J.O.P.M. NAKATA. Mechanical Stability of Mesoporous Materials, MCM-48 and MCM-41. 1999, **6**(1), pp.13-17.

63. DU, G., S. LIM, Y. YANG, C. WANG, L. PFEFFERLE and G.L. HALLER. Methanation of carbon dioxide on Ni-incorporated MCM-41 catalysts: The influence of catalyst pretreatment and study of steady-state reaction. *Journal of Catalysis*, 2007, **249**(2), pp.370-379.

Table 1.

Main possible reactions of pyrolysis- catalytic steam reforming-catalytic hydrogenation of biomass.

Reaction	Process (eq. no)
Pyrolysis Process (1st stage reactor)	
$Biomass \rightarrow H_2O + H_2 + CO + CO_2 + C_xH_yO_z + C_xH_y + Char$	Biomass pyrolysis (1)
Catalytic Steam Reforming Process (2nd stage reactor)	
$C_xH_yO_z \rightarrow H_2O + H_2 + CO + CO_2 + CH_4 + C_nH_m$	Catalytic tar cracking (2)
$C_xH_yO_z + H_2O \rightarrow H_2 + CO$	Tar steam reforming (3)
$C_nH_m + H_2O \rightarrow H_2 + CO$	Hydrocarbon steam reforming (4)
$C_xH_yO_z + CO_2 \rightarrow CO + H_2$	Tar dry reforming (5)
$C_nH_m + CO_2 \rightarrow CO + H_2$	Hydrocarbon dry reforming (6)
$CO + H_2O \rightarrow CO_2 + H_2$	Water gas shift reaction (7)
$2CO \rightarrow C + CO_2$	Boudouard reaction (8)
$C + H_2O \rightarrow CO + H_2$	Carbon steam gasification (9)
Catalytic Hydrogenation Process (3rd stage reactor)	
$CO_2 + 4H_2 \rightarrow CH_4 + 2H_2O$	CO_2 methanation reaction (10)
$CO + 3H_2 \rightarrow CH_4 + 2H_2O$	CO methanation reaction (11)
$C + 2H_2 \rightarrow CH_4$	Carbon hydrogasification reaction (12)

Table 2

Influence of catalytic steam reforming temperature on the product yield, gas ratios and gas composition (Pyrolysis temperature 800 °C, Steam WHSV 3 mL h^{-1} $g^{-1}_{catalyst}$.

	Catalytic Steam Reforming Temperature (°C)				
	600 (Sand)	600	700	800	900
Product Yield (wt. %)					
Gas	41.5	42.57	47.76	58.5	73.4
Solid (char)	19	19	20	20	20
Liquid (by difference)	38.5	37.43	32.24	21.5	6.6
Gas carbon content (wt.%)	26.66	25.12	29.03	35.74	45.45
Gas ratios					
H_2/CO	1.37	6.14	4.50	3.79	2.94
H_2/CO_2	1.22	4.95	4.78	3.7	3.19
CH_4/CO	0.47	0.14	0.03	0.04	0.008
CH_4/CO_2	0.42	0.11	0.03	0.04	0.009
CO/CO_2	0.88	0.80	1.06	0.98	1.08
Gas Composition (vol. %)					
H_2	33.4	72.0	70	64.8	60.4
CO	24.3	11.7	15.4	17.1	20.5
CO_2	27.4	14.5	14.5	17.4	18.9
CH_4	11.5	1.7	0.5	0.7	0.2
CnHm	3.3	0.1	0.2	0.1	N.D

*N.D- Not detectable

Table 3

Influence of catalytic steam reforming temperature on the product yield, gas ratios and gas composition (Pyrolysis temperature 800 °C, Catalytic steam reforming temperature 800 °C).

	Steam Weight Hourly Space Velocity (WHSV) (mL h^{-1} $g^{-1}_{catalyst}$)				
	1	3 (Sand)	3	5	9
Product Yield (wt. %)					
Gas	55.7	44.83	58.5	73.85	60.48
Solid (char)	20	20	20	20	20
Liquid (by difference)	24.3	35.17	21.5	6.15	19.52
Gas carbon content (wt.%)	35.34	31.29	35.74	43.41	41.04
Gas ratios					
H_2/CO	2.03	1.39	3.79	4.56	2.92
H_2/CO_2	3.95	1.514	3.7	2.80	1.88
CH_4/CO	0.013	0.039	0.04	0.056	0.47
CH_4/CO_2	0.02	0.042	0.04	0.034	0.30
CO/CO_2	1.93	1.089	0.98	0.614	0.64
Gas Composition (vol. %)					
H_2	57.2	41.4	64.8	63	48.6
CO	28.0	29.7	17.1	13.8	16.6
CO_2	14.4	27.3	17.4	22.4	25.7
CH_4	0.4	1.2	0.7	0.8	7.9
CnHm	N.D	0.4	0.1	0.1	1.2

*N.D- Not detectable

Table 4

Influence of catalytic hydrogenation temperature on the product yield, gas ratios and gas composition (Pyrolysis temperature 800 °C, Catalytic steam reforming temperature 800 °C, Steam WHSV5 mL h^{-1} $g^{-1}_{catalyst}$).

	3rd Stage Catalytic Hydrogenation Temperature (°C)			
	250	300	350	400
Gas Yield (wt. %)				
Gas (wt.%)	96.78	79.9	67.95	66.98
Gas carbon content (wt.%)	43.38	40.35	39.02	39.82
Gas ratios				
CH_4/CO	2.21	-	-	9.36
CH_4/CO_2	0.51	1.34	2.99	2.73
Gas Composition (vol. %) H_2 Free Basis				
CO	13.3	N.D	N.D	7.3
CO_2	57.2	42.6	25.0	24.8
CH_4	29.4	57.4	75.0	67.9
CnHm	0.1	N.D	N.D	N.D
Methanation H_2O (wt.%)	12	26	39	39

*N.D- Not detectable

Table 5

Influence of hydrogen space velocity on the product yield, gas ratios and gas composition (Pyrolysis temperature 800 °C, Catalytic steam reforming temperature 800 °C, Steam WHSV5 mL h^{-1} $g^{-1}_{catalyst}$, Catalytic hydrogenation temperature 350 °C).

	H_2 Space Velocity (mL h^{-1} $g^{-1}_{catalyst}$)			
	0	1200	2400	3600
Gas Yield				
Gas (wt.%)	60.78	59.8	61.97	67.95
Gas carbon content (wt.%)	42.82	38.19	41.11	39.02
Gas ratios				
CH_4/CO	1.79	-	-	-
CH_4/CO_2	0.45	1.84	3.17	2.99
Gas composition (vol. %)				
CO	14.9	N.D	N.D	N.D
CO_2	58.3	35.2	24.0	25.0
CH_4	26.8	64.8	76.0	75.0
CnHn	N.D	N.D	N.D	N.D
Methanation H_2O (wt.%)	12	26	39	37

*N.D- Not detectable

Table 6

Influence of 10 wt. % metal- alumina catalysts on the product yield, gas ratios and gas composition (Pyrolysis temperature 800 °C, Catalytic steam reforming temperature 800 °C, Steam WHSV5 mL h^{-1} $g^{-1}_{catalyst}$, Catalytic hydrogenation temperature 350 °C, Hydrogen space velocity 2400 mL h^{-1} $g^{-1}_{catalyst}$).

	Metal Catalysts				
	Sand	Ni/Al_2O_3	Co/Al_2O_3	Fe/Al_2O_3	Mo/Al_2O_3
Gas Yield (wt. %)					
Gas (wt.%)	81	61.97	64.7	85.15	77
Gas carbon content (wt.%)	39.01	41.11	40.85	38.7	35.96
Gas Ratios					
CH_4/CO	0.23	-	7.6	0.14	0.12
CH_4/CO_2	0.19	3.17	2.3	0.20	0.13
Gas Composition (vol. %) H_2 Free Basis					
CO	40.9	N.D	8.4	53.6	49.3
CO_2	48.8	24.0	27.6	38.5	44.3
CH_4	9.5	76.0	64.0	8.0	6.1
CnHm	0.8	N.D	N.D	N.D	0.2
Methanation H_2O (wt.%)	9	39	24	8	5

*N.D- Not detectable

Table 7

Influence of catalyst calcination temperature on product yield, gas ratios and gas composition (Pyrolysis temperature 800 °C, Catalytic steam reforming temperature 800 °C, Steam WHSV5 mL h^{-1} $g^{-1}_{catalyst}$, Catalytic hydrogenation temperature 350 °C, and Hydrogen space velocity 2400 ml h^{-1} $g^{-1}_{catalyst}$).

	Catalyst Calcination Temperature (°C)			
	650	750	850	950
Gas Yield (wt. %)				
Gas (wt.%)	61.05	61.97	59.7	63.58
Gas carbon content (wt.%)	40.89	41.11	40.64	39.99
Gas Ratios				
CH_4/CO	13.52	-	-	-
CH_4/CO_2	2.98	3.17	3.91	4.68
Gas Composition (vol. %) H_2 Free Basis				
CO	5.2	N.D*	N.D	N.D
CO_2	23.8	24.0	20.3	17.6
CH_4	70.9	76.0	79.7	82.4
CnHn	N.D	N.D	N.D	N.D
Methanation H_2O (wt.%)	37	39	39	39

*N.D- Not detectable

Table 8.

Influence of metal loadings on product yield, gas ratios and gas composition (Pyrolysis temperature 800 °C, Catalytic steam reforming temperature 800 °C, Steam WHSV5 mLh^{-1} $g^{-1}_{catalyst}$, Catalytic hydrogenation temperature 350 °C, and Hydrogen space velocity 2400 mL h^{-1} $g^{-1}_{catalyst}$).

	Catalyst Metal Loading (%)		
	5	10	15
Gas Yield (%)			
Gas (wt.%)	65.20	63.58	64.59
Gas carbon content (wt.%)	40.50	39.99	41.91
Gas Ratios			
CH_4/CO	11.89	-	9.47
CH_4/CO_2	2.21	4.68	2.55
Gas Composition (vol. %) H_2 Free Basis			
CO	5.5	N.D	7.1
CO_2	29.4	17.6	26.2
CH_4	65.2	82.4	66.8
CnHn	N.D	N.D	N.D
Methanation H_2O (wt.%)	33	39	34

*N.D- Not detectable

Table 9

Influence of different catalyst supports on product yield, gas ratios and gas composition (Pyrolysis temperature 800 °C, Catalytic steam reforming temperature 800 °C, Steam WHSV5 mL h^{-1} $g^{-1}_{catalyst}$, Catalytic hydrogenation temperature 350 °C, and Hydrogen space velocity 2400 mL h^{-1} $g^{-1}_{catalyst}$).

	Support Material		
	Al_2O_3	MCM-41	SiO_2
Gas Yield (%)			
Gas (wt.%)	63.58	79	87.88
Gas carbon content (wt.%)	39.99	43.99	44.53
Gas ratios			
CH_4/CO	-	2.4	0.58
CH_4/CO_2	4.68	1.06	0.77
Gas Composition (vol. %) H_2 Free Basis			
CO	N.D	17.7	34.7
CO_2	17.6	39.8	45.0
CH_4	82.4	42.5	20.2
CnHn	N.D	N.D	0.1
Methanation H_2O (wt.%)	39	16	10

*N.D- Not detectable

1149

1150 **FIGURE CAPTIONS**

1151

1152 **Figure 1**. Schematic diagram of the three stage (i) pyrolysis (ii) catalytic steam reforming
1153 (iii) catalytic hydrogenation reactor system

1154 **Figure 2** Influence of catalytic steam reforming temperature on gas yield (Pyrolysis
1155 temperature 800 °C, Steam WHSV3 mL h^{-1} $g^{-1}_{catalyst}$).

1156 **Figure 3** Influence of steam WHSVon the gas yield (Pyrolysis temperature 800 °C, Catalytic
1157 steam reforming temperature 800 °C).

1158 **Figure 4** Influence of catalytic hydrogenation temperature on the gas yield (Pyrolysis
1159 temperature 800 °C, Catalytic steam reforming temperature 800 °C, Steam WHSV5
1160 mL h^{-1} $g^{-1}_{catalyst}$).

1161 **Figure 5** Influence of hydrogen space velocity on the gas yield (Pyrolysis temperature 800
1162 °C, Catalytic steam reforming temperature 800 °C, Steam WHSV5 mL h^{-1} $g^{-1}_{catalyst}$,
1163 Catalytic hydrogenation temperature 350 °C).

1164 **Figure 6** Influence of 10 wt. % metal- alumina catalysts on gas yield (Pyrolysis temperature
1165 800 °C, Catalytic steam reforming temperature 800 °C, Steam WHSV5 mL h^{-1} $g^{-1}_{catalyst}$, Catalytic hydrogenation temperature 350 °C, and Hydrogen space velocity
1167 2400 mL h^{-1} $g^{-1}_{catalyst}$).

1168 **Figure 7** H_2 TGA-TPR of 10 wt. % Ni/Al_2O_3 catalysts calcined at various temperatures

1169 **Figure 8** Influence of catalyst calcination temperature on gas yield (Pyrolysis temperature
1170 800 °C, Catalytic steam reforming temperature 800 °C, Steam WHSV5 mL h^{-1} $g^{-1}_{catalyst}$, Catalytic hydrogenation temperature 350 °C, and Hydrogen space velocity
1172 2400 mL h^{-1} $_{catalyst}$).

1173 **Figure 9** SEM-EDXS analysis of various nickel loadings on alumina support a) 5 wt. %
1174 Ni/Al_2O_3 b) 10 wt. % Ni/Al_2O_3 c) 15 wt. % Ni/Al_2O_3.

1175 **Figure 10** XRD analysis of various nickel loadings on alumina support.

Figure 11 Influence of metal loadings on gas yield (Pyrolysis temperature 800 °C, Catalytic steam reforming temperature 800 °C, Steam WHSV5mL h^{-1} $g^{-1}_{catalyst}$, Catalytic hydrogenation temperature 350 °C, and Hydrogen space velocity 2400 mL h^{-1} $g^{-1}_{catalyst}$).

Figure 12 SEM-EDXS analysis of different catalytic supports a) 10 wt. % Ni/SiO_2 b) 10 wt. % Ni/MCM-41 c) 10 wt. % Ni/Al_2O_3

Figure 13 XRD analysis of 10 wt. % Nickel catalyst with different supports.

Figure 14 Influence of different catalyst supports on gas yield (Pyrolysis temperature 800 °C, Catalytic steam reforming temperature 800 °C, Steam WHSV5 mL h^{-1} $g^{-1}_{catalyst}$, Catalytic hydrogenation temperature 350 °C, and Hydrogen space velocity 2400 mL h^{-1} g^{-1} catalyst).

Figure 15. Comparison of the gas yields obtained from the two-stage and three-stage processes at the optimized conditions.